# Adhesion of soft solids in the presence of a thin fluid layer

*an attempt to model the curious features of insect adhesion*

Lennard van Buren

MSc thesis

August 5, 2016

PCC80436

Dr. MMG Kamperman
Supervisor
Wageningen University
Physical Chemistry and Soft Matter

Dr. D Labonte
Supervisor
Cambridge University
Department of Engineering

Prof.dr.ir. FAM Leermakers
Second examiner
Wageningen University
Physical Chemistry and Soft Matter

**Adhesion of soft solids in the presence of a thin fluid layer: an attempt to model the curious features of insect adhesion**

Dated August 5, 2016

Thesis submitted for the degree Master of Science (MSc)

*Lennard van Buren*

Author
Wageningen University
Student number: 930702146010
E-mail address: lennardvburen@gmail.com

*Dr. M.M.G. Kamperman*

Supervisor
Physical Chemistry and Soft Matter, Wageningen University and Research Centre, Wageningen, The Netherlands
E-mail address: marleen.kamperman@wur.nl

*Dr. D. Labonte*

Supervisor
Department of Engineering, Cambridge University, Cambridge, UK
E-mail address: david.labonte@eng.cam.ac.uk

*Prof.dr.ir. F.A.M. Leermakers*

Second examiner
Physical Chemistry and Soft Matter, Wageningen University and Research Centre, Wageningen, The Netherlands
E-mail address: frans.leermakers@wur.nl

# Abstract

Many insects use soft adhesive footpads to climb on plants. The adhesive contact of these footpads is mediated by a thin layer of an oily secretion, whose function remains largely unclear. Earlier work suggested that the fluid contributes to the adhesion via viscous dissipation, but this function has recently been questioned. In this study, we investigated in a simplified model system how the rate-dependence of wet soft adhesives was influenced by viscoelastic dissipation in the bulk solid versus viscous dissipation in the contact-mediating fluid layer. The rate-dependence of the adhesion of poly(dimethylsiloxane) (PDMS) followed an established empirical power law that links viscoelastic dissipation to crack propagation speed. When a liquid was present in the contact zone, the rate-dependence was reduced compared to dry contacts, but did not depend on the liquid's viscosity. This suggests that the contribution of dissipation via the liquid's viscosity was negligible, which is likely because the liquid was in "elastic confinement". Such a state of confinement is known to cause the liquid response to be dominated by deformation of the solid. We propose two mechanisms that may explain viscoelastic dissipation in the bulk solid in the presence of a fluid interface. In the first, the fluid is considered to act as a lubrication layer that limits viscoelastic dissipation near the crack tip, thereby decreasing rate-dependence of adhesion. In the second, rate-dependence is attributed to viscoelastic braking in a wetting ridge that emerges on soft solids as an effect of surface tension. Our results support the idea that the fluid layer in insect adhesion does not increase adhesion via viscous forces, but rather reduces rate-dependence by minimizing viscoelastic dissipation in the footpad.

# Preface

This thesis deals in fact with a very simple experiment: press a rigid ball in a droplet on a soft cushion, pull them apart again and measure how much force you need to do this. Especially with an experiment so simple, it is striking to find out how sophisticated the underlying behaviour is that governs the response. Do not all observables show the beauty of nature, where the laws of natural sciences come together to form one single unified response? For me, it is this combination of beauty and complexity that makes science so appealing.

I feel most indebted to several people who have helped in making this thesis both an interesting contribution to science and a valuable learning experience.

First and most of all, I wish to express my sincere gratitude to my two supervisors, Marleen Kamperman and David Labonte, for their guidance and support during my work. It has always been a pleasure working with you.

Marleen, thank you for putting trust in me. Your ever kindness and understanding makes you a fantastic and approachable supervisor, and I have learnt a great deal from you in the field of physical chemistry.

David, your dedication to this project has been determining for the outcome. Your almost instantaneous email replies have always kept me on the go, and you were always there to solve my lab problems. Furthermore, thank you for helping me in using R, ImageJ and LaTeX, and, not less important, for welcoming me in Cambridge and for the beers and discussions.

Many thanks go to Aljosha Fillipov for his patience in explaining physics to a non-physicist, and in helping a non-laboratorist with working in a chemical lab.

I am very grateful to Walter Federle for enabling me to do the force measurements in Cambridge, and to Aleksandra Birn-Jeffrey for her assistence in the lab in Cambridge.

Furthermore, I want to thank Joshua Dijksman for fruitful discussions and his help with the video analysis.

I feel indebted to Frans Leermakers and Jasper van der Gucht, for the discussions that were of great help.

Moreover, my gratitude goes to Stan Willems, for helping me in making the PDMS samples.

I want to thank all other people from the Insect Biomechanics Workgroup in Cambridge and the group of Physical Chemistry and Soft Matter in Wageningen, who have helped me with uncountable things.

Last, but not least, I feel indebted to all people who developed the open-source software that I used in this thesis: LaTeX, ImageJ and R.

# Contents

# 1 | Introduction

## 1.1 The insect wet adhesion mechanism

Climbing animals are able to climb on a variety of surfaces very well, ranging from smooth glass to rough rocks and from wet leaves to hydrophobic plants. Whereas the animals can easily grip on some surfaces by grasping around asperities with digits or by interlocking with claws, they have to "stick" to others [1]. For this last purpose, many animals use specialised adhesive footpads that comprise a wide set of requirements. The pads provide the animal with the capability to adhere to both hydrophilic and hydrophobic surfaces, to surfaces of different roughnesses and under different angles, combining strong attachment with rapid controllable detachment. The act of sticking is performed relatively effortlessly and can be repeated millions of times without losing functionality [2–5]. Although these specialized footpads have been subject to research for centuries [6, 7], their mechanism is still not completely understood, nor can their impressive combination of features be reproduced. As a result, both fundamental and applied scientists remain curious about the "sticky feet".

A first step in classifying these adhesive mechanisms is the distinction between "wet" and "dry" adhesion, where adhesive forces are believed to be generated by different interactions. Geckos and a variety of lizards would adhere directly with their feet to the surface; the so-called dry adhesion (see Figure 1a). The sophisticated ultrastructure of the feet enables numerous molecular contacts with the surface, leading to many intermolecular interactions such as van der Waals forces that, combined, generate a significant adhesive force [8].

On the other hand, tree frogs and insects use wet adhesion, where the contact between the pad and surface is mediated by a thin film of liquid that is excreted from the foot pad (see Figure 1b) [9–12]. The animals' sticking ability is often explained by a combination of the capillary and viscous forces arising from the fluid film [13–17]. Estimates for the thickness of the film go down to a few nanometers, thereby not excluding the possibility of additional "dry" intermolecular interactions between pad and surface [5, 9, 16].

Although the presence of a fluid film may increase the effective contact area and with that the total adhesive force on rough surfaces, additional fluid deposition on smooth surfaces would reduce any capillary and viscous forces as these decrease with fluid thickness [5]. The secreted fluid's exact function in the adhesive mechanism therefore remains largely unclear. Specific treatments to remove the secretion have been shown to reduce the insect's adhesive performance, but this

**(a)** **(b)**

**Figure 1: Dry and wet adhesion.** Animals make use of different types of specialized footpads to stick to a variety of surfaces. (**1a**) Geckos have adapted a dry adhesion mechanism, where the footpads adhere via numerous molecular contacts. Image obtained from Geckskin$^{\mathrm{TM}}$ (geckskin.umass.edu). (**1b**) Insects make use of wet adhesion. Here, we see the footpad of an ant with a fluid trail (blue). Credit: Walter Federle [5].

effect could not be decoupled from the dehydration of the pad, which by itself can lead to reduced adhesion [18, 19].

In order to describe the adhesive behaviour in the presence of a liquid film sandwiched between the pad cuticle and the surface, various models have been developed that consider the total adhesive force $F_{adh}$ to be the sum of capillary forces $F_{cap}$ and viscous forces $F_{vis}$ [12–17]:

$$F_{adh}(v) = F_{cap} + F_{vis}(v) \tag{1}$$

where $v$ is some characteristic speed involved in detachment. The contribution of the viscous force is rate-dependent, i.e. the faster one pulls, the higher the resistance of the viscosity. This behaviour is inherent to viscosity, hence viscous forces are a "dynamic" contribution to the adhesive force. On the contrary, capillary forces do not show a similar rate-dependent behaviour and generate a "static" force.

Recently, Labonte and Federle [12] have investigated the role of the secretion's viscosity in the wet adhesive behaviour of Indian stick insect foot pads. Although the adhesive force was indeed rate-dependent, the dynamic behaviour could not be explained by viscous effects in the fluid. Therefore, it was concluded that the contribution of the secretion's viscosity to adhesion was negligible. Instead, the authors suggested that the rate-dependence of adhesion resulted from dissipation in the pad cuticle.

In this new hypothesis for the role of the pad itself in wet adhesion we have found a starting point for the work presented here. However, insect footpads have a complex morphology, and many of the pad's properties are unkown. To accurately assess and describe the physics of a wet, yet soft adhesive contact, a simplified control system was used in this study. This artifical system allowed accurate control of the relevant properties and could be designed with a morphology amenable to first-principle mechanics. Furthermore, interest in the mechanics of soft solid materials has increased [20–22]. Most adhesive models work for either wet rigid materials [23, 24] or dry elastic materials [25, 26], but few exist that combine wet adhesion with elastic properties.

Therefore the following research question was phrased for this thesis:

*How does the presence of a thin fluid layer affect the adhesive behaviour of a soft solid?*

We note that the major goal of this study was of explorative nature. By combining expertise from physical chemistry and biomechanics, we have attempted to simplify insect adhesion to study the basic physics that govern the adhesive behaviour. In this way, we aimed to translate the mysteries of a complex biological system to simple, defined questions. The subquestions in this project were the following: What is the rate-dependence of adhesion of our artificial system without the presence of a liquid? How does the presence of a liquid affect this rate-dependence? What is the origin of rate-dependence in wet adhesion of soft solids?

The coming section summarises the theoretical framework that underlies our research question. After the introduction of the basics of insect adhesion, we continue with a short explanation of "dry fracture mechanics", the energy approach to the adhesive behaviour of soft solids. Next, we discuss the origin of rate-dependence of adhesion in these solids. Finally, we use this knowledge to motivate the design of our synthetic adhesive system chosen to address our research question.

## 1.2 The basis of dry fracture mechanics

The adhesive behaviour of soft solids was described by Barquins and Maugis in their dry fracture mechanics approach [25] and is shortly revisited in this section. We consider two solid elastic bodies that are in contact over an area $A$. Any variation in $A$ would change the total surface energy $U_S$, defined as

$$dU_S = (\gamma_1 + \gamma_2 - \gamma_{12})dA = -wdA \tag{2}$$

where, under true equilibrium conditions, $\gamma_1$ and $\gamma_2$ are the surface energies and $\gamma_{12}$ is the interfacial energy of the two bodies, and $w$ is the Dupré or thermodynamic work of adhesion. The total energy of the system $U_T$ under a load $P$ is the sum of the surface energy, stored elastic energy $U_E$ and potential energy of the load $U_P$, and its variation is, for an isothermal and reversible change, given by:

$$dU_T = dU_E + dU_P + dU_S \leq 0 \tag{3}$$

The strain energy release rate $G$ is now introduced, written as:

$$G = \frac{\delta U_E}{\delta A} + \frac{\delta U_P}{\delta A} \tag{4}$$

The variation of the total free energy in a spontaneous change can thus be written as:

$$dU_T = (G - w)dA \leq 0 \tag{5}$$

If $G = w$, the system is in equilibrium (Griffith's criterion). This equilibrium relation links $P$ to $A$ for equilibrium at fixed load. One might try to separate the bodies, i.e. to change $P$, which would via equation (4) translate to a change in $G$. According to equation (5), values $G > w$ force the system to decrease $A$, meaning that a separation of the two bodies is initiated. For the sake of simplicity, we assume here a circular contact zone. The receding contact area can be treated as a crack that propagates through the interface. The speed of crack propagation $v$ is defined as the change of contact radius $a$ with time $t$:

$$v = -\frac{da}{dt} \tag{6}$$

$G$ can be viewed as the energy required to extend an interfacial crack by a unit area, and a mechanical energy, $GdA$, is released when the crack extends by $dA$. The breaking of interfacial bonds requires the energy $wdA$ and the excess $(G - w)dA$ is either dissipated in the system or converted to kinetic energy. $G - w$ can be seen as the driving force for crack propagation, or the so-called crack extension force.

## 1.3 Rate-dependence in dry adhesion

In typical adhesion measurements, one measures this crack extension force $G$. The $G$'s obtained in measurements on elastomeric substrates are usually orders of magnitude higher than the thermodynamic work of adhesion [27], a result of the dissipative properties of the materials involved. This is explained as follows. The separation of the two surfaces occurs via the propagation of a crack through the interface. The highest strain rates are located near the crack tip where interfacial molecular interactions are broken (see Figure 2). For a moving crack the divergent strain field corresponds to a divergent strain rate [26]. When a crack propagates with a finite velocity, a region exists where the strain rate is high enough to trigger a viscoelastic response of the material: apart from a reversible stretching of the chains prior to seperation of the surfaces (the *elastic* response), segments from neighbouring molecules are now forced past one another, causing a molecular "friction" and, in turn, dissipation of energy (the *viscous* response [26, 28], see also Figure 2). The size of the region wherein this viscoelastic dissipation takes place depends on the strain rate and the properties of the material involved. So, while for lower crack propagation speeds the interfacial adhesion will dominate the crack extension force, higher speeds give rise to additional "bulk" effects. For the high crack propagation speeds that are reached in adhesion measurements, these bulk viscoelastic losses account for a significant part of the total adhesive force.

The combination of surface and bulk effects to adhesive force, whose specific contributions thus depend on crack propagation speed and material properties, has been captured for the adhesion of two solids by the following established power law [29–32]:

$$G = G_0 \left[1 + \left(\frac{v}{v^*}\right)^n\right] \tag{7}$$

where $G_0$ is the strain energy release rate ($\mathrm{mJ\,m^{-2}}$) as $v$ approaches zero,[1] $v^*$ is a characteristic crack speed where $G$ doubles with respect to $G_0$, and $n$ is an empirical constant that is often equal to 0.6 for elastomers [29, 31, 33].

In this relationship, $G_0$ accounts for the interfacial contribution to adhesion and can be viewed as the energy needed to break the bonds at the interface at thermodynamic equilibrium. When the work needed to separate the two interfaces is thermodynamically the same as the work needed to bring them together, $G_0 = w$. However, in the presence of strong interfacial bonds, $G_0$ is often found to significantly exceed $w$. Whereas the equilibrium *adhesion* energy $w$ is solely dependent on the surface energies of the bodies involved, the equilibrium *separation* energy $G_0$ depends on other factors, among which are cross-linking density [34, 35], interfacial bonding [26] and physical interactions [26, 36].

Additional bulk energy dissipation occurring within the system is accounted for by the second term between the brackets, which increases with the crack propagation speed. Note that bulk dissipation also depends on the interfacial adhesion energy via the multiplication factor $G_0$. As the rate-dependence of the crack propagation force is related to the viscoelastic properties of a material, the parameter $v^*$ is incorporated to account for this, with a low $v^*$ indicating a strong rate-dependence of $G$. Together, the empirical parameters $G_0$, $v^*$ and $n$ describe the combined contribution of bulk and surface effects in the adhesive force of viscoelastic solids.

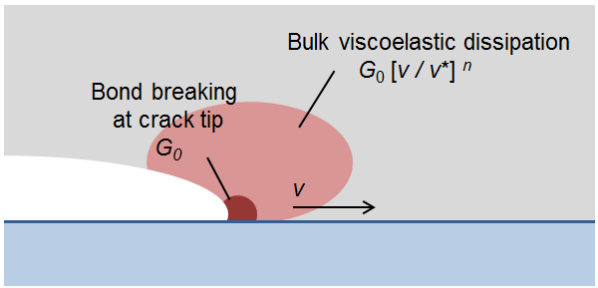


**Figure 2: Adhesive failure of viscoelastic materials.** A crack propagates through an interface between a viscoelastic material and a rigid solid with a finite velocity $v$. In the immediate vicinity of the crack, interfacial molecular bonds are broken (dark red). In a wider region, high strain rates give rise to viscoelastic dissipation (light red).

[1] For the sake of simplicity, we assume here that $G_0$ on itself is rate-independent. This is not true when energy is dissipated at the interface, e.g. in the case that covalent interfacial bonds are broken [26].

An addition to this theoretical understanding of the rate-dependence of adhesion comes from the work done by Ahn and Shull (1998) [30, 31]. They have shown that in the adhesion of two polymeric surfaces, an increased segmental mobility of interfacial chains reduces the rate-dependence of adhesion, i.e. leads to an increase of $v^*$ [31]. Segmental mobility is the ease with which a polymer chain can achieve different physical conformations. Polymers that are densely packed or that are below their glass transition temperature have a low segmental mobility. A high segmental mobility in the interface may give rise to a "lubrication effect" [36, 37], reducing energy dissipation in the bulk and thereby reducing the adhesion energies [31, 38]. Velocity dependence of the adhesion energy thus depends both on the bulk properties of the materials and on the segmental mobility in the interface - contributions of the bulk and of the interface can not be completely decoupled [26, 31].

## 1.4 A model system for insect adhesion

The outcomes of the experiments conducted by Labonte and Federle [12] suggest that insect wet adhesion follows a rate-dependence that takes the same form as the dynamic adhesion behaviour of elastomeric solids, with estimates for $n$ between 0.49 and 0.77 and $v^*$ between 37 and 13 $\mu m\,s^{-1}$. For elastomers, these parameters typically take values of about 0.6 [29] and from 0.1 to a maximum of 0.4 $\mu m\,s^{-1}$, respectively [27, 30, 31]. So it was noted that, while the rate-dependence of insect adhesion followed a similar trend as that for elastomers due to the similarity in $n$, the actual velocity-dependence was much lower in insect adhesion as evident from the higher $v^*$.

As we noted before, dissipative effects in adhesion may be minimized by a very mobile interfacial layer. Regarding the fact that wet adhesion of the insect footpads is mediated by a thin fluid layer and that the pads have viscoelastic properties [39], we might consider the insect wet adhesive system as a viscoelastic solid whose adhesion is mediated by a lubricating fluid layer. We therefore decided to model this adhesive system by using a soft elastomeric solid with a small volume of liquid deposited on the surface.

In this thesis we tried to approach a special case of soft solid adhesion, where the presence of a liquid gave rise to a mobile interface rather than dominating the overall system response. Performing "dry" adhesion tests allowed us to quantify the rate-dependence of the system in the absence of a fluid interface. To assess the influence of the fluid interface on rate-dependence of adhesion, we applied a small volume of liquid in the contact zone. We named these adhesion tests the "wet" adhesion experiments. Then, to gain more insight in the phenomena underlying rate-dependence, two liquids were tested that differed widely in viscosity.

# 2 | Materials and Methods

In this chapter, we first discuss how the soft solid samples were prepared. Then, we explain how samples were treated prior to wet adhesion measurements. We continue by discussing the setup and protocol that we used to measure the adhesion of the samples. The section ends with a part about the methods that we used to analyse rate-dependence of the dry and wet adhesives.

## 2.1 Sample preparation

As a model solid with well-defined properties, poly(dimethylsiloxane) (PDMS) was used (Sylgard 184, Dow Corning). The polymer, in the form of a silicone oil, was mixed with a cross-linking agent in a 20:1 (v/v) ratio, resulting in a Young's modulus of around 1 MPa [40–42], which is comparable to the estimates for the pads of stick insects (estimates around 100 kPa [43–45]). After stirring the mixture for 10 min by hand, the PDMS was degassed in a vacuum desiccator to remove air bubbles. The PDMS samples were required to have a thickness of about 400 µm in order to avoid sub-surface effects during indentation. A maximum thickness of 500 µm and a flat surface were required for visualization of the contact area (see below).

All samples were spin-coated to ensure flat surfaces and to control sample thickness [46]. The glass coverslips (18 mm × 18 mm × 0.14 mm) were first cleaned with acetone and demineralized water and subsequently dried at 80 °C. In order to ensure a sufficiently high viscosity of the mixed PDMS, the solution was left to "pre-cure" for 5 h prior to spin-coating. A droplet of PDMS was placed on a glass coverslip, then spin-coated at 300 rpm with an acceleration of 100 rpmps for 150 s. This combination of settings was found to be optimal as it ensured, next to the required layer thickness, complete spreading of the PDMS over the coverslip while limiting spin-off of the polymeric liquid.

Samples were cured overnight at 80 °C. The layer thickness, measured once for each sample (n=5) with a calliper, was $(0.41 \pm 0.03)$ mm. All adhesion experiments were done six weeks after preparation of the samples.

## 2.2 Sample treatment

For the wet adhesion tests, a small droplet of liquid was placed on top of the surface. In order to test the role of liquid viscosity, both pure and 1:1 (v/v) diluted glycerol were used. The two liquids have a comparable surface tension ($\gamma = 64.0\,\mathrm{mN\,m^{-1}}$

and $\gamma = 69\,\mathrm{mN\,m^{-1}}$ respectively, both at 20 °C) while the viscosity differs greatly ($\eta = 1.4\,\mathrm{Pa\,s}$ and $\eta = 8\,\mathrm{mPa\,s}$) [47, 48]. Droplets of both liquids were placed on the surfaces with a stretched glass capillary (2 µL, Hirschmann Laborgeräte, Eberstadt, Germany) connected to a manual pump.

The droplet volume was estimated by measuring the contact diameter of glycerol droplets on a glass coverslip one hour after placement, by assuming (i) a static contact angle of 38.3° [49], (ii) that a relaxation time of one hour allows full relaxation of the contact angle and (iii) that sessile droplets can be approximated as a spherical cap. The average droplet volume was $(10 \pm 2)$ nL (n = 10) - all values are (mean $\pm$ standard deviation), unless mentioned otherwise.

The PDMS surfaces were treated to ensure a low contact angle with a liquid that does not swell the elastomer, following the treatment protocol as described in ref. [50]. Samples were first immersed in 1 M NaOH for 24 h. Remaining NaOH was removed by rinsing the surfaces with demineralized water. When all remaining water droplets had evaporated, surface groups were modified with (3-aminopropyl) triethoxysilane (APTES) by chemical vapour deposition in a vacuum desiccator over 4 h with five droplets of APTES. Adhesion experiments were performed several days after the treatment.

The advancing and receding contact angles ($\theta_A$ and $\theta_R$, respectively) of diluted glycerol 1:1 (v/v) on APTES-treated PDMS surfaces were determined using the "conic section method" of Drop Shape Analysis (DSA for Windows, version 1.90.0.14, KRÜSS, Hamburg, Germany). A droplet was manually placed on the surface using a fixed syringe, and then either inflated or deflated to determine $\theta_A$ or $\theta_R$ respectively. The contact angle was measured at the moment the contact line started moving. Measured values were $\theta_A = (112 \pm 2)°$ and $\theta_R = (59 \pm 3)°$. Similar determination of $\theta_A$ and $\theta_R$ on untreated PDMS resulted in $\theta_A = (114 \pm 3)°$ and $\theta_R = 73°$ (n = 4 for all measurements). Contact angles for diluted and pure glycerol were assumed to be identical regarding the similarities in surface tension. Despite the small change in contact angle caused by the treatment, wetting properties of the sample were significantly changed upon treatment as appeared from contact area recordings (see discussion).

## 2.3 Force measurements

Adhesive forces were measured using a custom-built fibre-optic 1D-force transducer, described in ref. [12] (see Figure 3). Samples were placed with the PDMS oriented downwards in a sample holder that was attached to the end of a brass plate cut to 100 mm × 10 mm × 0.2 mm. A piece of reflective foil was glued to one end of the beam, close to the sample holder, while the other end of the beam was clamped onto a metal support. The support was fixed on a positioning stage equipped with a 3D motor (M-126PD, Physik Instrumente, Karlsruhe, Germany, resolution 0.25 µm, maximum velocity $15\,\mathrm{mm\,s^{-1}}$) and a 1D-piezo element (P-611.Z, Physik Instrumente, Karlsruhe, Germany, resolution 0.2 nm, travel range 100 µm) oriented to move in the Z-direction (normal to the surface). The positioning stage was

controlled by a custom-made LabVIEW software (National Instruments, Austin, TX, USA).

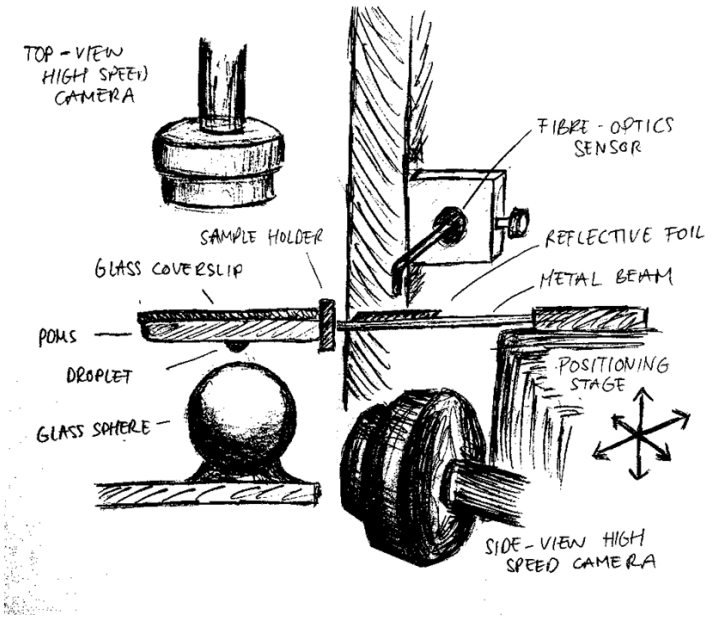


**Figure 3: Artist's impression of the setup used for force measurements.**

Perpendicular above the reflective foil, a D12 fibre optics sensor (Philtec, INC., Annapolis, USA) was placed. The intensity of the light detected by the sensor changed with the distance between foil and sensor. This intensity was converted to a voltage, which was thus a measure for the distance between the sensor tip and the beam. Using the stiffness[1] of the beam $k_m = 157\,\mathrm{N\,m^{-1}}$, distance was related to force. The sensor's sensitivity varied with the distance between sensor tip and reflective site, being highest in the middle of the linear near-field region (see data sheet, ref. [51]). The end of the sensor was lowered towards the reflective foil using a micro-manipulator placed on a custom-built holder. Using the built-in amplification factor of the sensor's amplifier, the optical peak of the sensor was set to 5 V. The sensor was then further lowered towards the middle of the linear near-field region, which corresponded to a force of 0 mN.

For an adhesion test, the sample was brought into contact with a spherical glass probe (diameter 4.78 mm) until a pre-defined load of $(1.0 \pm 0.1)$ mN was reached, which was maintained by a feedback-control loop for about 20 s. Then, a retraction was performed with an upward movement of the piezo element with one of the eight speeds given in Table 1. At the end of the run, motor and piezo were moved back to their initial position. During the entire load-unload cycle, the force output signal of the fibre-optic sensor was collected via a data acquisition board (PCI-635E, National Instruments) with a frequency of 50 Hz which was used by LabVIEW for

[1] The stiffness of the beam depends on the leverarm, which was held constant over all experiments.

the force-feedback loop. A 50 Hz output signal containing motor position was collected simultaneously. Furthermore, a 1000 Hz signal was streamed using a 2020 PicoScope oscilloscope (Pico Technology Ltd, Neots, Cambridgeshire, UK), which was used to extract force data for analysis. For retraction speed 0.01 $\mu m\,s^{-1}$ the oscilloscope recorded with 100 Hz.

**Table 1:** Overview of retraction speeds and corresponding video recording rates.

| Retraction speed in $\mu m\,s^{-1}$ | Frames per s |
|---|---|
| 0.01 | 1 |
| 0.1 | 5 |
| 1 | 25 |
| 10 | 196 [a] |
| 50 | 196 [a] |
| 100 | 196 [a] |
| 200 | 392 [a] |
| 500 | 392 [a] |

[a] For retraction speeds with a frame rate higher than 100 frames per second, side-view recordings were performed with 98 frames per second, a restriction imposed by the maximum recording rate of 100 Hz of the Basler camera.

During detachment both top- and side-view recordings of the adhesive contact were made. The top-view recordings were made using a TTL-triggered Redlake PCI 1000B B/W high-speed camera (Redlake MASD LLC, San Diego, CA, USA), mounted on a stereo-microscope with coaxial illumination (Wild M3C, Leica, Wetzlar, Germany). Top-view images showed the contact area throught the PDMS. Surface flatness was required to maximize contrast. The maximum focal depth of the camera was around 500 µm, meaning that this was the maximum sample thickness that could be used. A TTL-triggered Basler A602f B/W high-speed camera (Basler Vision Technologies, Ahrensburg, Germany) recorded the adhesive contact from the side.

Table 1 shows the frame rate of the recordings for the different retraction speeds. Trigger signals for both Basler and Redlake camera recordings were generated with LabVIEW for the three slowest retraction speeds. In order to allow synchronization of the video frames with the force trace, the trigger signals were also recorded with the oscilloscope. Problems in signal transfer between the LabVIEW software and cameras occurred with frame rates higher than 100 Hz. Therefore the setup was not suited to make recordings with the higher frame rates. As an alternative, these higher speed recordings were triggered with a strobe (Drelloscop 2009AN, Drelloscop, Germany, maximum frequency 417 Hz) while the oscilloscope recorded the strobe trigger signals. Notwithstanding, data analysis showed that strobe signals as collected by the oscilloscope did not have the ex-

pected frequency, thereby hindering synchronization of force and video recordings for retraction speeds higher than $1\,\mu m\,s^{-1}$.

Indentations were performed both with a glass sphere on APTES-treated PDMS samples (the dry adhesion tests) and with a glass sphere on a droplet of liquid on treated PDMS samples (the wet adhesion tests). For the dry adhesion tests, the sphere had been in contact with treated PDMS for numerous times before the first experiment was done without being cleaned in between, to prevent effects of the transfer of free oligomers on adhesion, as described in ref. [52]. Load-unload cycles were performed with all retraction speeds in a random order on a single spot on the treated surface. After every eight indentations, the sphere was moved to a new spot and the load-unload cycles were repeated in a random order. In this way, every retraction speed was tested nine times, with indentations on three different spots on three different surfaces.

The procedure for performing the wet adhesion tests was slightly different from the one for dry adhesion tests. Every wet adhesion test started with the placement of a droplet, and it was ensured that the adhesion experiments were initiated within 30 min after the droplet was placed. The first five indentations on a droplet showed a changing spreading behaviour accompanied by an increasing force. After five indentations, spreading and force became constant for repeated indentations. For these reasons five load-unload cycles were performed on every new droplet before measurements were performed. The retraction speed $0.01\,\mu m\,s^{-1}$ was only performed thrice with diluted glycerol, all other retraction speeds were performed nine times for all other samples. All measurements were performed at ambient conditions (22–25 °C, 40–55 % relative humidity) to avoid a systematic influence of temperature or humidity on adhesion.

## 2.4 Data analysis

Force data was extracted from the oscilloscope signal using R 3.3.0 [53]. The resolution of the oscilloscope signal for retraction speeds 0.01, 0.1 and $1\,\mu m\,s^{-1}$ was higher than required and was downsampled by selecting every i-th value to frequencies 2 (i = 50), 10 (i = 100) and 20 Hz (i = 50), respectively. The force-time traces were used to (i) determine the peak adhesive froce $P_c$ and (ii) construct force-displacement curves.

First, the peak adhesive force $P_c$ was determined by applying a second order LOESS smoothing algorithm, span = 0.05, and then finding the maximum value of this LOESS curve.

Subsequently, force-time traces were coupled to their corresponding displacement in the following way. The indentation depth of the sphere in the PDMS ($\delta$) during load was determined from the LabVIEW data. The start of the indentation ($\delta = 0$) was derived from the moment when the first repulsive force was measured. This point was defined as the point where the next subsequent 20 force measurements were all lower than the 20 preceding data points. From the motor position ($\Delta$) at the start of indentation ($\Delta = 0$), the motor decreased further until the system reached a repulsive force of 1 mN. The motor position corresponding to

the indentation depth during this preload was found by taking $\Delta$ averaged over the last 20 data points before the start of the retraction movement. Relaxation effects of the PDMS were found to have an insignificant influence on the motor position during this preload. It should be noted that this procedure only worked for dry adhesion measurements as for wet adhesion measurements there was no clear event in the force trace when the sphere started indenting the PDMS. It was therefore not possible to obtain force-displacement data for these experiments.

Continuing from the start position of the motor, the movement of the positioning stage was modelled with the piezo retraction speed. Since the beam used in our experiments was found to have a finite stiffness compared to the adhesive site, any movement of the positioning stage led to a competition between retraction of the sphere and bending of the beam. A correction for this elastic displacement of the beam was proposed by Barquins and Maugis [25]:

$$\Delta = \delta + \delta_m = \delta + \frac{P}{k_m} \tag{8}$$

where $\delta_m$ is the displacement of the beam and $P$ the normal force acting on the tip of the beam. Using this relationship, we were able to calculate the actual position of the sphere and thus to relate force to displacement.

### 2.4.1 Rate-dependence in dry adhesion

For dry adhesion measurements, we treated the decreasing contact radius as a crack as defined in equation (6). The crack propagation speed $v$ will be called $v_{cd}$ henceforth, and the dry contact radius will be named $a_d$ throughout this thesis. To obtain $a_d$, top-view video recordings were post-processed using ImageJ 1.44n [54] (see appendix for videos). First, recordings were converted into binary images using an "IsoData" algorithm, after which the native particle detection routine was applied. Of the detected particles, the feret diameter was measured which was divided by two to obtain the contact radius. A second order LOESS-algorithm (span = 0.7) was applied to smooth the contact data. To compensate for the decrease in resolution with increasing detachment speed, the LOESS-algorithm was used to predict the contact radius at 10 Hz between the measured points. With these predicted values, the crack propagation speed was then obtained using the contact radii at the moment of peak adhesion and one data point, corresponding to 0.1 s, after that. It was not possible to synchronize the strobe signal with the force data with sufficient accuracy. Therefore, crack propagation speeds at the moment of peak adhesion could only be obtained for the lowest three retraction speeds.

Rate-dependence of dry adhesion was assessed by estimating the parameters $n$ and $v^*$ via two different routes which are described below.

(i) *Relating peak adhesive force to relative energy dissipation*

For defined geometries, relative adhesive forces can be related to the relative dissipation, which is basically equation (7) rewritten as:

$$\frac{G}{G_0} - 1 = \left(\frac{v_{cd}}{v^*}\right)^n \tag{9}$$

For a spherical indenter, $G/G_0 = P_c/P_0$ [12, 55], where $G$ and $P_c$ are the strain energy release rate and peak adhesive force at the finite crack propagation speed $v_{cd}$, respectively, and $P_0$ is the equilibrium pull-off force. Equation (9) was fitted to the data by first averaging values of $v_{cd}$ and $P_c$ per retraction speed. Then, the averaged $P_c$ and $v_{cw}$ for the lowest two retraction speeds were linearly extrapolated to obtain a pull-off force under equilibrium conditions ($v_{cd} = 0$), yielding $P_0 = 1.0\,\text{mN}$. The parameters $v^*$ and $n$ were fitted to the averaged data using a non-linear least squares algorithm.

(ii) *Fitting Barquins and Maugis differential equations*

For every experiment, the evolution of $P$, $a_d$ and $\delta$ was predicted over time using their corresponding differential equations as described by Barquins and Maugis [25]. Then, using a non-linear least squares algorithm, the parameters $v^*$, $n$ and $G_0$ were fitted. We describe the procedure here in more detail.

For a rigid sphere with radius $R$ in contact with an elastic half space with Young's modulus $E$, we assume that the displacement of the sphere $\delta$ as a function of applied force $P$ follows Johnson-Kendall-Roberts (JKR) theory, meaning that [56]:

$$\delta = \frac{a_d^2}{3R} + \frac{2P}{3a_d K} \tag{10}$$

where $a$ is the contact radius and the reduced modulus $K$ is defined as $1/K = 3(1-\nu^2)(4E)^{-1}$. Following JKR theory, $G$ is given by:

$$G = \frac{3a_d^3 K}{8\pi R^2}\left(1 - \frac{R\delta}{a_d^2}\right)^2 \tag{11}$$

At equilibrium, $a_0$ under a load $P_0$ is given by [56]:

$$a_{d0} = \left(\frac{P_0 R}{K}\left[1 + \frac{3\pi w R}{P_0} + \left(\frac{6\pi w R}{P_0} + \left[\frac{3\pi w R}{P_0}\right]^2\right)^{1/2}\right]\right)^{1/3} \tag{12}$$

where $w$ is the thermodynamic work of adhesion. The displacement velocity of the sphere $\dot{\delta}$ follows the displacement speed of the piezo $\dot{\Delta}$ (note that this is equal to what we have called the retraction speed) via equation (8) and equation (10):

$$\dot{\delta} = \frac{d\delta}{dt} = \frac{1}{1 + \frac{3a_d K}{2k_m}}\left[\dot{\Delta} - \frac{3K}{2k_m}\left(\delta - \frac{a_d^2}{R}\right)\frac{da_d}{dt}\right] \tag{13}$$

Before, we assumed that the strain energy release rate $G$, at a finite crack propagation speed $v_{cd}$, is the sum of a rate-independent and a rate-dependent term (equation (7)). We use this equation together with equations (10) and (11) to find the speed of crack propagation:

$$\dot{a_d} = v_{cd} = \frac{da_d}{dt} = -v^* \left[ \frac{3a_d^3 K}{8\pi R^2 G} \left( 1 - \frac{R\delta}{a_d^2} \right)^2 - 1 \right]^{1/n} \tag{14}$$

Note the negative sign in equation (14): an advancing crack corresponds to a receding contact area. The evolution of force is then given by:

$$\dot{P} = \frac{dP}{dt} = \frac{3}{2} K \left( \delta \dot{a_d} + \dot{\delta} a_d - \frac{a_d^2 \dot{a_d}}{R} \right) \tag{15}$$

The differential equations (13) to (15) were used to predict the evolution $\delta$, $P$ and $a_d$ for the different retraction speeds. Initial values for $\delta$ and $a_d$ were derived from equations (10) and (12). Specifying parameters $\dot{\Delta}$ as the respective retraction speed, $P_0 = 1\,\text{mN}$, $K = 16/9\,\text{MPa}$, $k_m = 157\,\text{N m}^{-1}$ and $R = 2.39\,\text{mm}$ allowed us to fit parameters $G_0$, $v^*$ and $n$ using experimental data obtained for $P$ and $\delta$. This fitting procedure will be called the Barquins and Maugis fitting procedure henceforth. Note that, while the evolution of all three states $\delta$, $P$ and $a_d$ was predicted, only two states ($P$ and $\delta$) were used for fitting. The frequency of the experimental data was decreased ten-fold prior to fitting to speed up analysis. The model required upper and lower boundaries and starting values for the parameters to be fitted, which we changed between different fitting trials (see results section) [30, 31, 33].

### 2.4.2 Wet adhesion

During contact area recordings in wet adhesion experiments, we observed three different regions as shown in Figure 4a: a light surroundings (the dry PDMS), a grey area and a darker region within this grey area (see discussion for further explanation, see appendix for videos). The size of the dark area decreased during the retraction movement. In analogy to the dry crack propagation speed, we defined a wet "crack propagation speed":

$$v_{cw} = -\frac{da_w}{dt} \tag{16}$$

where $a_w$ is the square root of the dark area. Video recordings were processed using a custom-made Matlab script (Matlab R2015b, The Mathworks, Natick, MA, USA). Images were first de-speckled with a $6 \times 6$ Gaussian filter. They were then converted to binary images using the native thresholding algorithm. Of the detected region (see Figure 4b), the major and minor axis and area were determined. Of all wet adhesion experiments, only several indentations on four different droplets (one

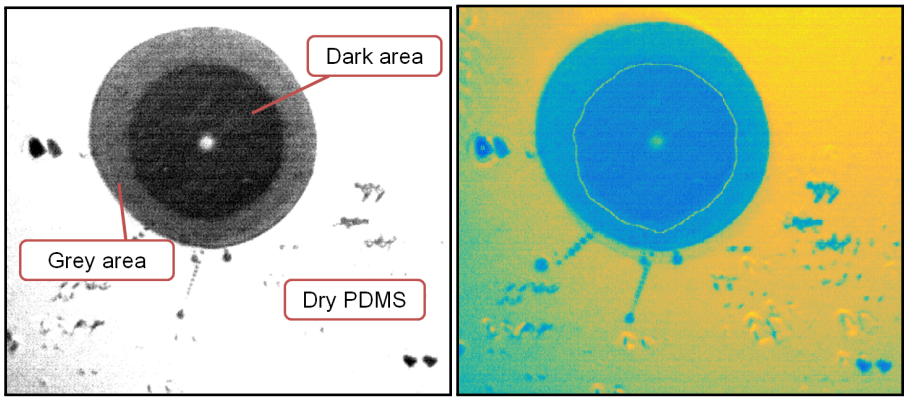


**Figure 4: Wet contact area images.** The image was taken at the end of the retraction movement of a wet adhesion test with glycerol, retraction speed $1\,\mu m\,s^{-1}$ . (**4a**) Image of the contact area. Contrast and brightness were adjusted for visualization purposes. The light region indicates dry PDMS surface. Within the grey region, a circular shaped darker region is visible. A reflection of the glass sphere is seen in the middle of the dark area as a small light spot. (**4b**) Output of the same image when processed for determination of the size of the dark area. The yellow line indicates the perimeter of the detected region.

for glycerol, three for diluted glycerol) were found to be suitable for this analysis. In the other videos, the contrast between the dark area and the grey surrounding was too poor to detect the perimeter of the dark area. Since the droplet did not always spread to a circular area (major axis was up to 1.4 times as long as minor axis), an effective radius was approached by taking the square root of the measured area. $v_{cw}$ was determined manually by drawing a tangent to the square root of the area over time, at the point right before the "collapse" in contact occurred (dotted line in Figure 7, see further explanation in results section). $v_{cw}$ was not used for quantitative comparisons.

# 3 | Results

## 3.1 Rate-dependence of dry adhesion

Forces recorded for dry adhesion experiments collapsed to zero after having reached a peak adhesive force $P_c$ (or started oscillating around zero for retraction speeds $> 100\,\mu m\,s^{-1}$). See Figure 5a where a force-time curve is shown for a retraction speed of $1\,\mu m\,s^{-1}$. Figure 6 shows that $P_c$ strongly increased with retraction speed by a factor of eight. At $0.01\,\mu m\,s^{-1}$, representing a quasi-equilibrium detachment, the adhesive force was $P_c = (1.07 \pm 0.13)\,mN$, while $P_c$ increased up to $(9.01 \pm 0.35)\,mN$ for a retraction speed of $500\,\mu m\,s^{-1}$ (both values are mean $\pm$ standard deviation, $n = 9$).

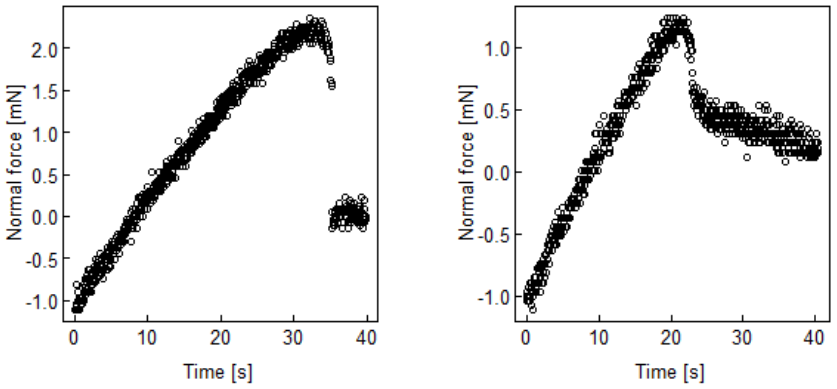


**Figure 5: Characteristic force curves for a single dry and wet experiment.** Both experiments were conducted with a retraction speed of $1\,\mu m\,s^{-1}$. (**5a**) Dry adhesion experiment. The adhesive force increased to a peak value and then dropped to zero. (**5b**) Wet adhesion experiment with glycerol present in the contact zone. The adhesive force increased to a peak value, then dropped to a positive value and followed a slow decrease from that point on.

Figure 7 shows how the contact area changed during the retraction movement. In the dry adhesion experiments, the receding contact area suddenly collapsed, leading to complete detachment of the sphere from the PDMS surface. The speed

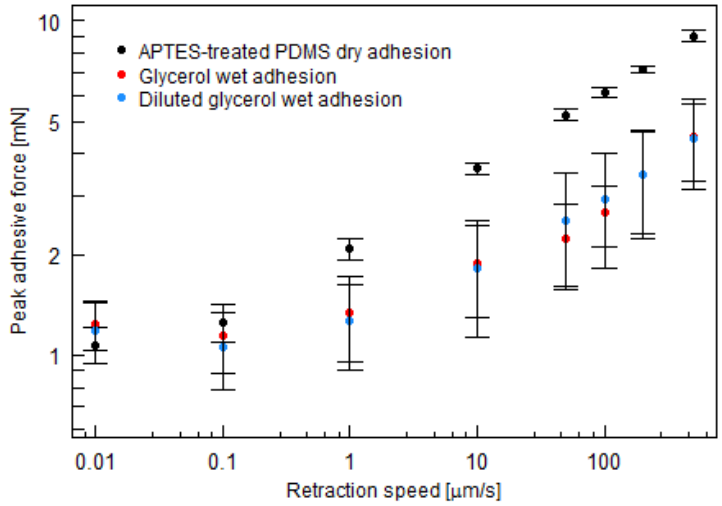


**Figure 6: Variation of peak adhesive force with retraction speed for dry and wet adhesives.** Plotted on a log-log scale. Error bars show mean $\pm$ standard deviation (n = 9). While adhesive forces for dry and wet adhesives were comparable at lower speeds, they differed for higher retraction speeds. Across four orders of magnitue, dry adhesive forces increased by a factor eight, while wet adhesive forces only increased by a factor four.

of crack propagation $v_{cd}$ at the moment of peak adhesion increased over two orders of magnitude with retraction speed as depicted in Figure 8a.

The variation of the relative crack extension force $G/G_0 - 1$ with $v_{cd}$ is shown in Figure 9 together with a fit of equation (9) (black dashed line). The fit was obtained by a non-linear least-squares algorithm with the assumption that the contact can be modelled as a spherical indenter on an elastic halfspace. The fit yielded $n = 0.63$ and $v^* = 8.88\,\mu m\,s^{-1}$ (95 % confidence intervals (0.49, 0.76) and (7.73, 10.04), respectively). Fixing $n$ at 0.6, which is common practice when considering elastomeric solids [29, 31, 33], led to a similar estimate of $v^*$.

Using the Barquins and Maugis fitting procedure to fit the parameters $n$, $v^*$ and $G_0$ led to reasonably good fits with the experimental data for the lowest retraction speed (see Table 2, RMSE = 0.18). The pull-off force obtained by linear extrapolation ($P_0 = 1.0\,mN$) was used as a starting value of $88\,mJ\,m^{-2}$ for $G_0$ (see discussion how $G_0$ was calculated from $P_0$). The starting values for $v^*$ and $n$ ($0.15\,\mu m\,s^{-1}$ and 0.6, respectively) were based on literature values for elastomer adhesion [26, 29, 31]. Fitting with the experimental data obtained at higher retraction speeds led to increased errors (see discussion). Therefore, only results for the lowest retraction speeds were used for fitting the differential equations. When $n$ was fitted, we obtained estimates for $n$ and $v^*$ comparable to the results obtained by fitting equation (9) (see Table 2). Fixing $n$ at 0.6 while using the same starting values as above resulted in fits with similar estimates, but with increased error (see

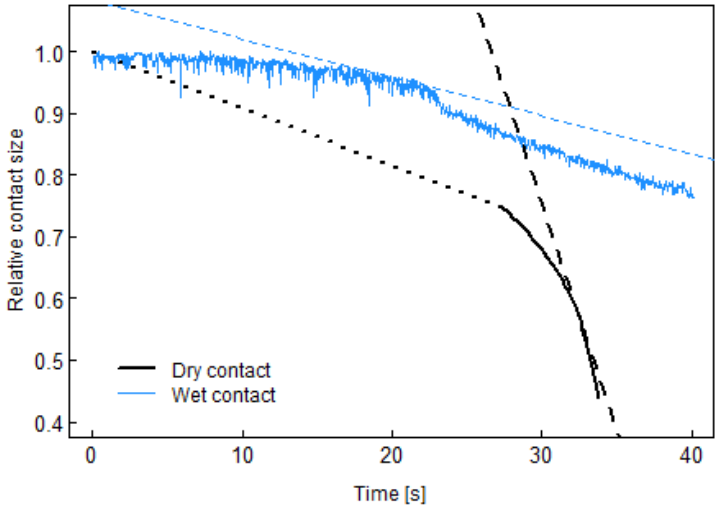


**Figure 7: Dry and wet relative "contact" evolution over time.** Contact data was extracted from the same experiments as the force trace and images in Figures 4 and 5. The black solid line shows the decrease of the relative dry contact radius. A manually measured contact radius at the start of the experiment (0.18 mm) was added and connected to the other measurements with a straight dotted blue line to give a better idea of the complete detachment process. The black dashed line indicates $v_{cd}$. The blue solid line gives the square root of the wet "contact" area over time. The contact area decreased continuously (square root of initial area was 0.8 mm), then "collapsed" and eventually followed again a steady decrease. A (manually derived) tangent was added right before this collapse to show how $v_{cw}$ was determined.

Table 2). Furthermore, a starting value of $G_0$ of 58 mJ m$^{-2}$, which is close to the APTES surface energy (see discussion), with fixed $n$, resulted in fits with a significantly lower $v^*$, but the fits were poor (see Table 2 and red dashed line in Figure 9).

## 3.2 Rate-dependence of wet adhesion

Whereas the force measured in dry adhesion experiments rapidly dropped to zero after the peak adhesion was reached, in the presence of a liquid in the contact zone this drop stopped at a non-zero adhesive force (Figure 5b). From this point onwards, the force steadily decreased. When the same wet adhesion experiments were carried out with longer force recordings, i.e. over a longer retraction distance, this decrease continued until the adhesive force was 0 mN (data not shown). Side-view recordings of the contact zone revealed that this slow decrease in force was accompanied by slow stretching of the liquid bridge connecting indentor and surface, but that no clear event in the force trace was associated with the breaking of

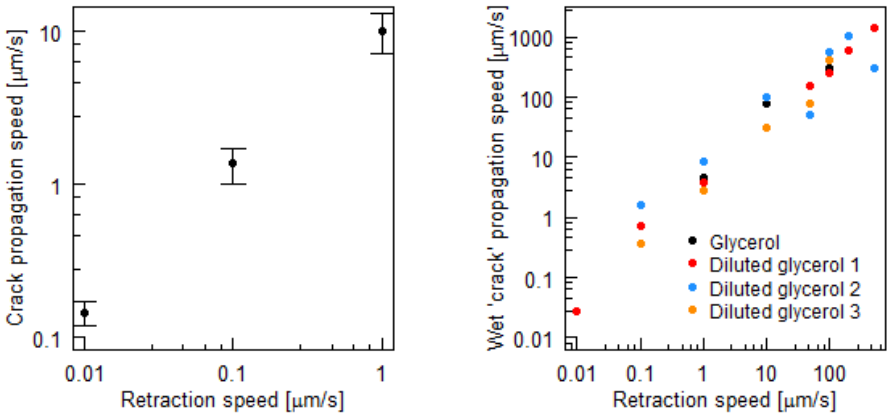


**(a)** **(b)**

**Figure 8: Influence of retraction speed on dry and wet "crack propagation speeds".** Plotted on a log-log scale. Error bars show mean ± standard deviation. (**8a**) Dry crack propagation speeds taken at the moment of peak adhesion. $v_{cd}$ increased over two orders of magnitude with increasing retraction speed. (n = 9) (**8b**) Wet "crack propagation speed", determined as discussed in Figure 7. $v_{cw}$ could be determined for four samples. "Diluted glycerol X" contains measurements performed with a set of retraction speeds on droplet X. The numbers do not indicate different dilutions.

the bridge. This final steady decrease was only observed for lower retraction speeds ($< 100\,\mu m\,s^{-1}$), as for the highest retraction speeds the beam started oscillating heavily after the force drop, without breaking the liquid bridge.

In the presence of a liquid droplet in the contact zone, the increase of adhesive forces with retraction speed was only fourfold, or half as high as for dry contacts. When the liquid was glycerol, the measured peak adhesive forces ranged from (see Figure 6) $(1.24 \pm 0.21)$ mN and $(1.19 \pm 0.25)$ mN for retraction speeds 0.01 and $0.1\,\mu m\,s^{-1}$, respectively, to $(4.49 \pm 1.17)$ mN for the highest retraction speed (n = 9 for all [1]). Performing the same experiments with diluted glycerol resulted in peak adhesive forces of $(1.19 \pm 0.25)$ mN for $0.01\,\mu m\,s^{-1}$ (n=3), $(1.06 \pm 0.28)$ mN for $0.1\,\mu m\,s^{-1}$ (n=9) and $(4.46 \pm 1.35)$ mN (n=8) for $500\,\mu m\,s^{-1}$. Despite an almost 200-fold difference in viscosity between the two liquids, the dependence of the adhesive force on retraction speed did not differ significantly (two-way ANOVA, $F_{1,129} = 0.55$, $p = 0.905$, $n = 18$). Furthermore, we note that the variation in peak adhesive force is significantly higher than for dry adhesion (see error bars in Figure 6).

[1] Data on retraction speed $0.1\,\mu m\,s^{-1}$ was included because the sample size for this retraction speed was higher than for $0.01\,\mu m\,s^{-1}$ for measurements with diluted glycerol (n = 9 and n = 3, respectively).

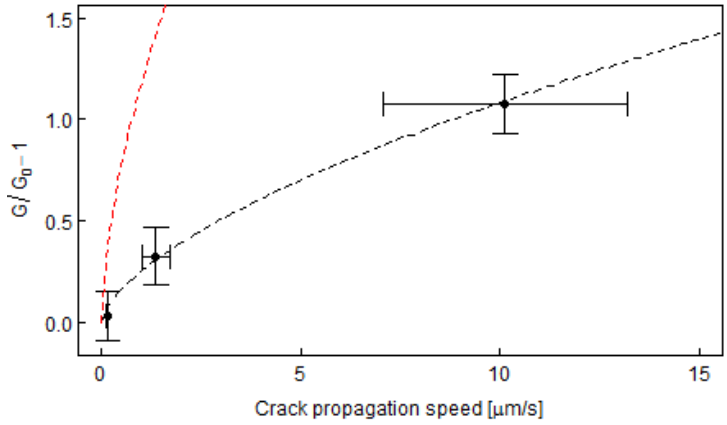


**Figure 9: Relationship between relative crack extension force and crack propagation speed in dry adhesion.** Error bars show mean ± standard deviation. The black dashed line represents the empirical power law (equation (9)) that was fitted through the data, with $P_0 = 1.0\,\text{mN}$, $v^* = 8.88\,\mu\text{m}\,\text{s}^{-1}$, $n = 0.63$. The red dashed line is the result of the Barquins and Maugis fitting procedure with $G_0 = 62\,\text{mJ}\,\text{m}^{-2}$, $v^* = 0.42\,\mu\text{m}\,\text{s}$, $n = 0.6$ (see discussion).

The video frame in Figure 4 is the top-view image corresponding to the end of the retraction movement of the experiment shown in Figure 5b. During the recording (see appendix), the perimeter of the lighter grey region (Figure 4a) stayed more or less constant. The dark area, on the other hand, initially overlapped with the grey area, but decreased in size during retraction. The relative evolution of the square root of this dark area (see Figure 4b for detected region) over time is depicted in Figure 7. A retraction movement started with a slowly receding dark area, until the area suddenly "collapsed" to a lower (non-zero) value, and finally followed a steady decrease. Note that the final decrease in dark area (after the collapse) occurs with a higher speed than the initial decrease. All recordings for wet adhesion experiments showed a behaviour similar to the characteristic behaviour described here, albeit with differing geometries of the grey and dark areas (see materials and methods). Comparing the contact area evolution with the force trace showed that the collapse in contact area coincides with the drop in force after peak adhesion. Using the slope of the tangent as drawn in Figure 7 (blue dotted line), we obtained an estimate for $v_{cw}$. $v_{cw}$ is thus the wet crack propagation close to peak adhesion. $v_{cw}$ increased with retraction speed over several orders of magnitude (one-way ANOVA, $F_{1,21} = 30$, $p < 0.001$, $n = 4$, see Figure 8b), for both viscosities in a similar fashion (two-way ANOVA, $F_{1,19} = 0.14$, $p = 0.716$, $n = 4$). Peak adhesive force increased with $v_{cw}$ (one-way ANOVA, $F_{1,21} = 28$, $p < 0.001$, $n = 23$, see Figure 10).

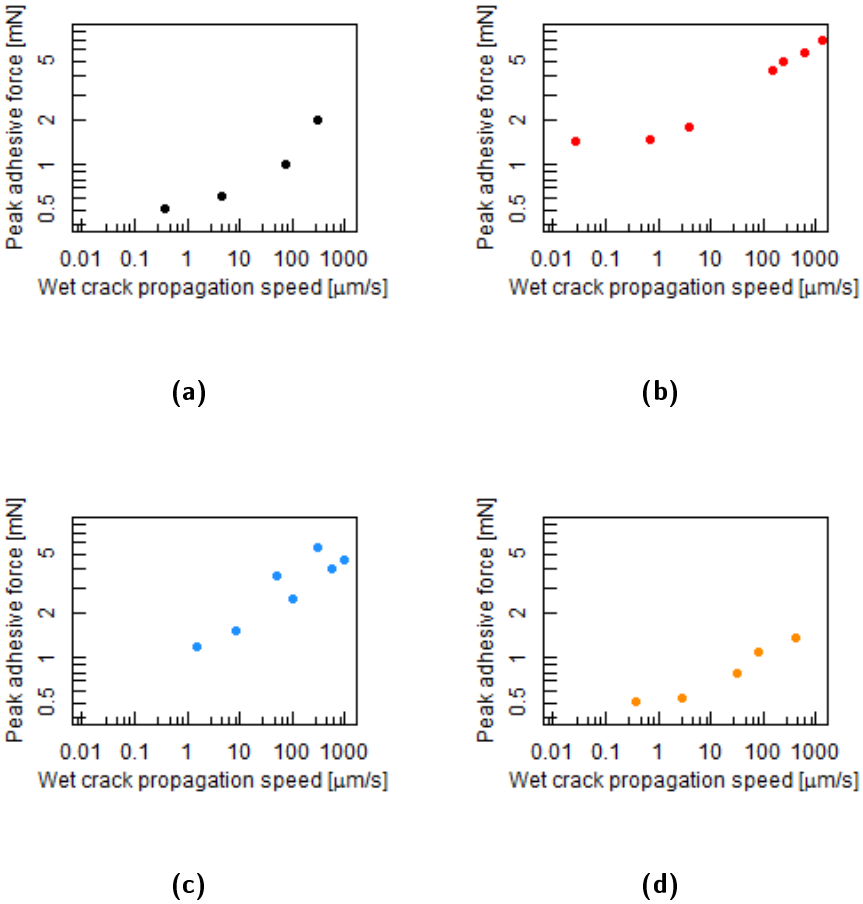


**Figure 10: Peak adhesive force versus wet "crack" propagation speed.** Peak adhesive force increased with wet crack propagation speed for all four droplets. **(10a)** Glycerol. **(10b, 10c, 10d)** Diluted glycerol.

**Table 2: Fitting results of parameters $n$, $G_0$ and $v^*$ using the Barquins and Maugis fitting procedure.** The two lowest retraction speeds were used for fitting, with $n$ either fixed or allowed to fit. Estimates are mean $\pm$ standard deviation, $G_0$ in [mJ m$^{-2}$], $v^*$ in [µm s$^{-1}$] (n = 7 for retraction speed 0.01 µm s$^{-1}$ and n = 9 for 0.1 µm s$^{-1}$).

| Retraction speed in µm s$^{-1}$ | Parameter | Lower boundary | Upper boundary | Starting value | Estimate |
|---|---|---|---|---|---|
| 0.01 | $n$ | 0.5 | 0.75 | 0.6 | 0.68 $\pm$ 0.11 |
| | $G_0$ | 80 | 96 | 88 | 82.6 $\pm$ 5.7 |
| | $v^*$ | 0.01 | 9 | 0.15 | 8.89 $\pm$ 0.07 |
| | RMSE[a] | | | | 0.18 $\pm$ 0.05 |
| 0.1 | $n$ | 0.5 | 0.75 | 0.6 | 0.69 $\pm$ 0.11 |
| | $G_0$ | 80 | 96 | 88 | 82.2 $\pm$ 5.1 |
| | $v^*$ | 0.01 | 9 | 0.15 | 8.90 $\pm$ 0.08 |
| | RMSE | | | | 0.39 $\pm$ 0.17 |
| 0.01 | $n$ fixed | - | - | - | 0.6 |
| | $G_0$ | 80 | 96 | 88 | 86.5 $\pm$ 8.6 |
| | $v^*$ | 0.01 | 9 | 0.15 | 6.0 $\pm$ 4.1 |
| | RMSE | | | | 0.35 $\pm$ 0.04 |
| 0.01 | $n$ fixed | - | - | - | 0.6 |
| | $G_0$ | 56 | 65 | 58 | 62.2 $\pm$ 3.6 |
| | $v^*$ | 0.01 | 1 | 0.15 | 0.42 $\pm$ 0.39 |
| | RMSE | | | | 0.38 $\pm$ 0.11 |

[a] Root mean square error

# 4 | Discussion

Wet and soft adhesives are ubiquitous in nature, yet little is understood about their detailed functioning. A question that remains is how soft footpads interact with a liquid film to achieve a highly controllable adhesion. Previous research was ambiguous, with some saying that the fluid increases adhesion via viscosity, and others speculating that the fluid may reduce the rate-dependence of adhesion. The latter is also suggested by the outcomes of our experiments. Our study revealed that rate-dependence of wet adhesives can be independent of the fluids viscosity, suggesting that dynamic adhesion is not an effect of viscous dissipation in the liquid. This section starts with relating our results on dry adhesion to literature data. Then, several mechanisms are discussed that may have been the origin of a different rate-dependence in the wet adhesion data. The first mechanism considers the rate-dependence as an effect of viscous dissipation in the liquid. The next two mechanisms consider rate-dependence as an effect of viscoelastic losses in the soft solid. Finally, we relate our findings to the wet adhesion of insect footpads.

## 4.1 Rate-dependence in dry adhesion

### 4.1.1 Static detachment

In the limit of low crack propagation speeds, the contribution of viscoelastic dissipation to the pull-off force should be negligible. For these quasi-equilibrium detachments in a sphere-on-flat geometry at fixed load, the pull-off force $P_0$ is given by JKR theory as [56]:

$$P_0 = \frac{3}{2}\pi R w \tag{17}$$

where $R$ is the radius of the sphere and $w$ is the thermodynamic work of adhesion. Note that this relation takes the pull-off force to be directly dependent on the work of adhesion, i.e. the work required to adhere and separate the surfaces is identical. Using $R = 2.39\,\mathrm{mN}$ and assuming $w$ to be equal to the surface energy of APTES, which is $61\,\mathrm{mJ\,m^{-2}}$ [57, 58], we obtain $P_0 = 0.7\,\mathrm{mN}$. We use the surface energy instead of the work of adhesion, as to our knowledge no comparable work of adhesion has been reported for glass and APTES surfaces. This prediction is comparable to the experimental equilibrium pull-off force that we obtained by linear extrapolation of the lowest two adhesive forces towards $v_{cd} = 0\,\mu\mathrm{m\,s^{-1}}$ (0.7 vs 1.0 mN, see materials and methods). When we use equation (17) to calculate an equilibrium pull-off force using $G_0 = 82\,\mathrm{mJ\,m^{-2}}$, which we obtained with the Barquins and Maugis fit-

ting procedure, a quasi-equilibrium pull-off force of 0.92 mN is obtained. This is in good agreement with the quasi-equilibrium pull-off force that we obtained via equation (9) (0.92 vs 1.0 mN).

The calculated $G_0$ is higher than the surface energy of APTES (82 vs 61 mJ m$^{-2}$). Such an overestimation of $G_0$ with respect to $w$ is often found for adhesion of polymers [59]. As mentioned before (see introduction), the equilibrium separation energy $G_0$ depends on more factors than the surface energy alone.

From the above, we conclude that static detachment in dry adhesion experiments follows predictions from JKR theory, albeit with a discrepancy introduced by a fundamental difference between $w$ and $G_0$ .

### 4.1.2 Rate-dependence

At higher retraction speeds, adhesive forces of the dry contacts increased. Quantification of the rate-dependence resulted in estimates for $v^*$ and $n$ that were consistent for the two fitting procedures applied (relative crack extension force fitting: $v^* = 8.88\,\mu m\,s^{-1}$, $n = 0.63$; Barquins and Maugis fitting procedure: $v^* = 8.89\,\mu m\,s^{-1}$, $n = 0.68$). Our estimates of $n$ are close to the literature value of 0.6 that is widely used to describe elastomeric behaviour [30, 31, 33]. The estimates for $v^*$ are significantly higher than has been reported for PDMS in literature (215 nm s$^{-1}$ [31]) and are, in fact, higher than all other values that have been found for elastomers, which typically go up to 0.4 µm s$^{-1}$ [27, 31, 32, 60, 61]. Possibly, the pre-treatment of PDMS has changed the viscoelastic properties of the elastomer that might translate into a change of any of the above variables. Moreover, detachment was recorded at retraction speeds that were significantly higher than those applied by previous authors [27, 31]. A different explanation for this discrepancy may be found by having a more detailed look at the specific fitting procedures.

We note first that the prediction of independent values of contact radius $a_d$, using $P$ and $\delta$ and the Barquins and Maugis fitting procedure (see methods) resulted in outcomes that were in good agreement with the experimentally obtained values for $a_d$. From this we conclude that contact area measurements were reliable and that our estimate for the elastic modulus $E$ (1 MPa) was close to the experimental value. However, especially for higher retraction speeds, errors diverged during the fitting procedure, and (one or more of) the estimates ended up at the specified boundaries. Besides this, the experimental force-displacement data used for the fitting procedure had an insecurity on itself. This insecurity is caused by the determination of "zero indentation depth", i.e. the point where the sphere started indenting the soft surface, which is subject to error (see materials and methods). It has been shown that precise surface detection is crucial for achieving accurate indentation results, especially for compliant materials [62]. The success of the Barquins and Maugis fitting procedure turned out to be strongly dependent on starting values and set boundaries. When all three parameters $G_0$, $n$ and $v^*$ were fitted, we used a starting value for $n$ of 0.6, as reported in literature, and the

outcome of the other fitting procedure as a starting value for $G_0$. This approach resulted in a relatively high $v^*$ (see Table 2). By fixing $n$ at 0.6, as has been done before in literature to obtain estimates for $v^*$ [29, 31, 33], fitting resulted in estimates for $v^*$ and $G_0$ that were much closer to literature values. However, a fit with comparable error was found with a much higher $G_0$ and $n$. The model thus seems to be undertermined with respect to fitting of the paramters. It can be noted that fitting equation (9) with $n$ fixed at 0.6 leads to a similar estimate for $v^*$ as varying $n$. We ascribe this to the limited number of data points that was used for this fitting procedure. Together, the above suggests that multiple fits could be obtained with different estimates for $G_0$, $v^*$ and $n$. The detailed reasons underlying these variations and the underdetermination of the fits requires further detailed experiments.

The obtained rate-dependence of the dry adhesives follows the established empirical power law in equation (7), but with a higher estimate for $v^*$ than has been reported in literature.

## 4.2 Wet adhesion mechanism

### 4.2.1 Viscous dissipation in the fluid

Figure 6 shows that in the presence of a liquid, peak adhesive forces were less dependent on retraction speed than they were for dry contacts. We note that the variation of measured forces was high between the different droplets (see error bars for wet adhesion in Figure 6 compared to dry adhesion). However, measurements one single droplet gave consistent results. Video recordings showed that different droplets spread to different "squeezed" orientations and the droplet volume may have changed between experiments as fluid transfer did not only involve a consistent volume that was taken up inside the capillary, but also a changing fluid volume that adhered to the exterior of the capillary. For these reasons, we attribute the variation in peak force to a variation both in droplet volume and spreading behaviour.

According to the simple "wet adhesion model", the dynamic component in wet adhesion arises from viscous effects, whereas capillarity forms the static contribution to the adhesive force (see equation (1)). When this wet adhesion model is applied to our artificial system, we can predict the static pull-off force by only taking into account the capillary contribution. Considering a capillary bridge between a sphere and a flat soft surface, the static adhesive force is given by [23]:

$$P_0 = P_{cap} = 3\pi R\gamma \cos\theta \tag{18}$$

in which $\gamma$ is the surface tension of the liquid and $\cos\theta$ is the average of the cosines of the contact angles $\theta_1$ and $\theta_2$ of the liquid with the plane and the sphere, respectively [24]. Due to the similarities of their surface tensions [63], we assume the contact angles of pure and glycerol to be identical. For an adhesion mediated by glycerol, $\gamma = 69\,\mathrm{mN\,m^{-1}}$ and the contact angle of glycerol on glass $\theta_2 = 38.3^\circ$ [49]). The receding contact angle of diluted glycerol on APTES-treated PDMS ($\theta_1$) was

measured to be 59°. Therefore, the predicted adhesive force[1] is 1.35 mN versus an average force of 1.01 mN measured in our experiments (95 % CI (0.82, 1.66) at retraction speed 0.01 µm s$^{-1}$). This suggests that the static adhesive force can be explained by capillary forces.[2]

Despite a two hundredfold difference in viscosity between the two liquids, we measured no influence of viscosity on adhesive force. The estimated viscous contribution to the adhesive force[3] can be found by [64]:

$$P_{vis} = 6\pi R^2 \frac{\eta}{h}\left(\frac{dh}{dt}\right) \tag{19}$$

where $\eta$ is the viscosity of the fluid, and $h$ is the fluid film thickness underneath the centre of the sphere.[4] The viscous force is dependent on the separation speed $dh/dt$ between the two solid surfaces, which we approximate with the applied retraction speed. For the viscous force of diluted glycerol to amount 3.5 mN at a retraction speed of 500 µm s$^{-1}$ (see Figure 6: forces increase from about 1 mN to about 4.5 mN), $h$ should be around 100 nm ($\eta = 0.008$ Pa s). A similar viscous force in an undiluted glycerol liquid bridge ($\eta = 1.4$ Pa s) is achieved with a liquid layer thickness of 20 µm. It should be noted that at higher speeds, the retraction speed can be an overestimation of the actual separation speed, a result of the deformation of the beam.

The liquid thickness in our system is estimated following Martin and Brochart-Wyart [65]. For a liquid film intercalated between a spherical rubber lens and a flat rigid plate, the film thickness under the centre of the sphere over time $h(t)$ can be approached with a classic Reynolds law via:

$$h(t) = \frac{b}{\sqrt{t}} \tag{20}$$

Here, $b$ is a constant (ms$^{-1/2}$) that depends on the deformed flat area of the lens with radius $a$. Although our system consists of a rigid sphere on a soft half space, the relationship between contact area and external force is via Hertz theory identical as in ref. [65]. A difference exists in the fact that our contact site shows a curvature due to the rigid spherical indenter, whereas the contact area was flat in ref. [65]. We believe the effect of this discrepancy to have a minor influence on the squeeze-out behaviour, and therefore use the same expression for $b$, being:

$$b = \sqrt{\frac{27\pi}{64}\frac{\eta R a}{E}} \tag{21}$$

[1] It should be noted that by making this prediction, we implicitly assume that there are no additional interfacial forces playing a role besides capillarity, so adhesive force as a direct result of surface tension and any solid-solid interactions between PDMS and sphere are discarded.

[2] A static contact angle for diluted glycerol on APTES-treated PDMS was not measured. When the capillary force was calculated with a static contact angle instead of a receding contact angle, the estimated force would be smaller, bringing experimental and theoretical values closer to each other.

[3] In this relationship, both sphere and plane are assumed to be rigid.

[4] We assumed here that $h << R$.

From contact area recordings of wet contacts, PDMS deformation could not be derived, as will be discussed later. We therefore assume that the deformed region of the PDMS during load in wet adhesion is similar to the one measured in dry adhesion, i.e. $a = 0.2\,\text{mm}$.[5] With $E = 1\,\text{MPa}$, $R = 2.39\,\text{mm}$, we obtain after 20 s equilibration time a layer thickness $h$ of 15 nm for diluted glycerol ($\eta = 8\,\text{mPa s}$) and $h = 200\,\text{nm}$ for glycerol ($\eta = 1.4\,\text{Pa s}$).

So, the liquid layer appears to be much thinner than predicted from a viscous contribution to adhesive force. The above reasoning leads to a significant overestimation of the theoretical viscous contribution compared to the experimental results (overestimation of factor 30 for diluted glycerol, factor 100 for pure glycerol). The measured rate-dependence of adhesion can thus not be attributed to viscosity.

An explanation for this can be found in the confinement of the liquid: liquids that are subject to geometric constraints on a nanometer scale show a behaviour deviating from their bulk response. Confined liquids tend to "solidify", having an apparent viscosity much higher than their bulk viscosity [66, 67]. Their behaviour may even shift from a viscous to an elastic response [68]. Whereas thicker liquid layers lead to full lubrication where adhesion is only determined by viscosity and capillarity, confinement of the liquid may cause the overall response to be dominated by the solid [69, 70].

Villey et al. [70] found that when the film thickness is below a critical fluid film thickness $h_c$, the liquid is in elastic confinement. In that case, the overall response of the liquid becomes dominated by elastic deflections of the solid. We approximate our system as an oscillating drainage flowas in ref. [70], where a fluid is confined between a rigid sphere and a rigid plane. The relative distance between the two surfaces is varied harmonically with a frequency $\omega/2\pi$. In that case, the critical thickness is given by [70]:

$$h_c \approx R \left( \frac{\omega \eta}{K} \right)^{2/3} \tag{22}$$

where $R$ is the radius of the sphere and $K$ is the reduced elastic modulus. Using $\omega = v/h_c$, $K = 1.78\,\text{MPa}$, $v = 500\,\mu\text{m s}^{-1}$, the critical thickness is of the order 5 µm for glycerol ($\eta = 1.4\,\text{Pa s}$) and of the order 0.6 µm for diluted glycerol ($\eta = 8\,\text{mPa s}$). Note that $h_c$ decreases with decreasing retraction speed. From this state of confinement, we derive that the apparent viscosity of the confined fluid was higher than its bulk viscosity. Although this might have limited squeeze-out via equations (20) and (21), this effect would only be present when the liquid *is* in confinement. As a result, it is not necessary to take into account the effect of the increased viscosity on the state of confinement.

Concluding, the fluid was in elastic confinement ($h < h_c$): estimates for $h_c$ are orders of magnitude higher than the estimated fluid thicknesses. A liquid response dominated by solid behaviour explains why rate-dependence of wet adhesion was independent of the liquid's viscosity. Although a possible overestimation of the

[5] Note that this is much smaller than the initial dark area observed in wet experiments (radius around 0.8 mm). Interpretation of this dark area will be discussed on page 30.

separation speed in equation (19) may have misguided our estimation for the viscous force in our system, estimates for $h_c$ confirm that a viscous response was not dominant. So, as the liquid's viscous contribution to adhesion is apparently minimal, an alternative "energy sink" causing rate-dependence of adhesion is found in the viscoelastic PDMS.

### 4.2.2 Viscoelastic dissipation in the soft solid

In this section, two possible mechanisms that may explain viscoelastic dissipation in the PDMS in the presence of a thin interfacial fluid layer are discussed. Neither of the two is able to fully explain the behaviour of the wet adhesives, as will be explained below. After introducing the respective mechanism, an attempt is made to explain the characteristic force curve (see Figure 5b) in light of this mechanism. Both sections end with a note about general assumptions that were made.

Before continuing with the outcomes of our experiments, it is useful to discuss an experiment performed by Zhang et al. (2010) [71]. The authors tested the adhesive force between a plate and a sphere fixed on a cantilever. Both plate and sphere were rigid, made of glass and silicium nitride, respectively, while the cantilever was soft. Similar to our experiments, a movement of the cantilever in the normal direction was followed by an adhesive force. By changing the amount of fluid in the contact zone by a so-called "drop splitting method", the authors were able to measure adhesive forces in the presence of a picoliter volume of liquid. From their experiments, we learn three interesting things. First, a large sudden decrease in adhesive force was accompanied by a sudden "shrinking" of the liquid. This combination of effects, i.e. a drop in force with a shrinking liquid contact area, shows a striking parallel with our experimental outcomes for wet adhesion. Second, a further increase in interfacial clearance caused a slow and steady decrease in adhesive force, akin to the last part of the force trace in Figure 5b. Third, the "shrinking release force" was only present when the fluid was confined below a certain volume. The latter might indicate a relationship between elastic confiment and an observed force drop.

#### Mechanism 1: Crack propagation through a mobile interfacial layer

In elastomer adhesion, an increased segmental mobility of the interfacial chains is known to reduce the rate-dependence of adhesion [31]. Since the relaxation times of polymers are dependent on their surrounding medium [28, 72], the highly mobile fluid may have led to an increased interfacial mobility (see Figure 11a). Thus, we consider the system to be similar to a dry adhesive, albeit with a very mobile interface. It should be noted that this mechanim can only explain our data if forces are transmitted through the fluid layer. This may either occur because of polymer chains penetrating through the fluid layer to be in contact with the indenter, or because of confinement effects of the fluid layer.

Before we explain the force trace with this mechanism, let us first discuss in more detail the top-view recordings that were made during the experiments. We note that the existence of the "grey" area (see Figure 4a) was accompanied by two

observations: (i) liquid spreading on treated surfaces always followed the emerged grey area, whereas the wetting path on untreated surface was more random; (ii) a similar grey area was absent upon repeated indentations on untreated surfaces. These two observations suggest that treatment caused the surfaces to adsorb a thin fluid layer, the "grey area". This observation is consistent with literature: polymer chains have been reported to "trap" thin fluid layers with thicknesses in the order of the polymer chain length [73–75]. The darker area within the wetted area had a sharp edge (see Figure 4); the interpretation of the dark area and the edge differ per mechanism discussed. Although the presence of a circular dark area during preload may suggest that this dark area was an effect of PDMS deformation induced by the sphere, the dark area remained after the sphere and the surface were visibly separated. In fact, the dark area was also present when only a sessile droplet was present on the surface. The rim of the dark area can therefore be interpreted as the result of a finite contact angle between a macroscopic droplet and the prewetted surrounding region. A similar coexistence of a microscopic thin fluid film with a macroscopic droplet has previously been reported in cases of partial wetting [76–78]. However, it can not be excluded that in some stages during the load-unload cycles the dark area was only an effect of PDMS deformation. Since these different interpretations determine the plausibility of the two mechanisms that will be discussed, the precise interpretation of the dark area will be considered for each mechanism separately.

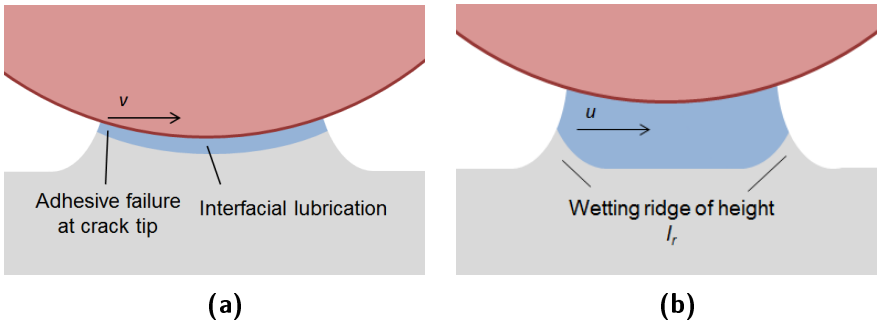


**Figure 11: Two possible mechanisms for viscoelastic dissipation in the presence of a fluid layer.** Rigid indenter in red, fluid in blue and PDMS in grey. No interpretation was made for liquid spreading outside the contact zone. (**11a**) Mechanism 1: crack propagation through a mobile interface. The fluid layer is treated as a mobile interfacial layer that decreases viscoelastic dissipation in the soft solid through lubrication. A crack propagates with a velocity $v$ through the fluid layer. (**11b**) Mechanism 2: viscoelastic braking. A wetting ridge of height $l_r$ is pulled up at the contact line as an effect of surface tension. Dislocation of the wetting ridge with a finite speed $u$ causes energy dissipation in the solid.

We now relate four events in the force trace (Figure 5b) to our observations and interpretations.

(i) *Increasing force caused by viscous and elastic response:* The first increase in force is, according to this mechanism, an effect of the viscous and elastic response of the PDMS when a crack propagates through the interface between the probe and the liquid/PDMS. Additional adhesive forces, e.g. capillary forces, are considered to be negligible.

(ii) *Peak adhesion when crack propagation becomes unstable:* Following this approach, peak adhesion is reached when crack propagation becomes unstable, i.e. when $\delta G/\delta A < 0$ [79]. Note that up to here, the detachment procedure is identical as to dry adhesion, and dissipation arises from high strain rates at the crack tip.

(iii) *Force drop as interfacial chains are detached or liquid escapes confinement:* In line with the above, the unstable crack propagates increasingly fast, which would lead to a sudden inwards flow of the liquid, possibly preceded by detachment of the interfacial chains from the indenter. Where in dry adhesion the force dropped to zero at this point, the fluid layer may have prevented this by forming a capillary bridge, which we explain as follows. We observed that the force drop was accompanied by a "collapse" in dark area (Figure 7). Preservation of volume dictates that this collapse must have been accompanied by a jump in interfacial clearance, i.e. an increase in distance between the probe surface and the PDMS surface. In turn, the liquid layer thickness may even have increased above $h_c$, meaning that it was no longer in elastic confinement and that a capillary bridge may have formed connecting the solid surfaces. The capillary adhesive force may have caused the jump to stop. A similar phenomenological explanation may be derived for the force drop that occurred for small liquid volumes that occurred during the experiments in ref. [71]: when the liquid was initially in elastic confinement, a consecutive big increase in interfacial clearance favoured the formation of a stable capillary bridge. As the tests in ref. [71] were performed with a silicium nitride indenter and a glass surface, the force drop in those experiments can not be explained by detachment of interfacial chains. This favours the hypothesis that the force drop is an effect of the sudden increase in fluid layer thickness, and that chain penetration is not necessary to allow force transmission through the fluid layer.

(iv) *Decreasing force due to stretching a capillary bridge:* At the end of the trace, we observed a force that decreased slowly and rather monotonously with time. Side-view recordings showed a liquid film that was stretched in the normal direction in this late stage of the retraction movement. In agreement with a liquid being no longer in elastic confinement, we suggest that capillary forces dominate the force response in this stage. The force of a capillary bridge

between a sphere and a plane as a function of clearance reads [80]:

$$P = \frac{3\pi R\gamma \cos\theta}{1 + h/d} \tag{23}$$

where $d$ is the sagitta[6] of the wetted part of the sphere and $h$ is the film thickness under the center of the sphere. Side-view recordings suggested a wetted radius of the sphere of 0.84 mm right after the force drop and 0.64 mm at the end of the retraction movement. With $R = 2.39$ mm, this leads to $d = 37$ µm and $d = 22$ µm, respectively. Right after the force drop, using $P = 0.5$ mN (see Figure 5b), $\gamma = 69$ mN m$^{-1}$, $\theta_1 = 59°$, and $\theta_2 = 38.3°$, we estimate a film thickness of $h = 32$ µm. At the end of the retraction movement, $P = 0.2$ mN, leading to $h = 81$ µm. The time between both points was about 18 s, meaning that the piezo displacement was 18 µm (retraction speed 1 µm s$^{-1}$). Taking into account effects of beam bending on interfacial clearance and the inaccuracy in determination of $d$ and the contact angles, capillary forces might have had a dominant contribution in this late stage of detachment.

We note that the end of the force curve is in our experiments similar as in the experiments performed by Zhang et al. (2010) [71]. The authors also proposed the stretching of a capillary bridge to cause the final decrease in force.

It should be taken into account that above explanation can only account for the observed rate-dependence if either the chains could penetrate through the liquid layer, or if forces could be transmitted through the liquid layer due to its confinement. Both confinement and chain penetration require the layer to be very thin, i.e. of microscopic thickness. The dark area observed in the top-view recordings can therefore not be interpreted as a continuous liquid layer of macroscopic thickness. According to this mechanism, the dark area may have been a result of deformation of the PDMS surface caused by the sphere. It is not excluded that this deformation was accompanied by a macroscopic fluid film around the "confined contact zone".

In order to assess the plausibility of force transmission between the interfaces, we first have a closer look at chain penetration through the fluid layer. We defined two major prerequisities for this to occur. One, the liquid layer should be thin enough for chains to span it, and two, penetrating the liquid layer should be energetically favourable. Assuming a polymer chain length in the order of tens of nanometers, these chains may penetrate the diluted glycerol layer with an estimated thickness of 10 nm, but spanning the 150 nm thick glycerol layer seems less likely. Quantitative comparisons should be treated with care as the calculation of thickness may deviate from the real fluid thickness, due to the fact that equation (21) does not necessarily have to hold due to the various approximations involved.

Crossing a hydrophilic fluid layer may not be favourable for hydrophobic PDMS chains, but possibly the APTES-treatment was not limited to the chain ends at

[6] The sagitta of a circular arc is the distance from the center of the arc to the center of its base.

the surface, i.e. hydrophilization may have occurred over a longer chain length, thereby making further penetration of the layer more likely. It is possible to develop a different argument considering the energetic favourability of chains penetrating the liquid layer when taking into account that contact between sphere and PDMS requires a local dewetting of the two surfaces. The stability of the liquid film between the glass sphere and treated surface depends on the sign of the spreading coefficient, which is given by [81]:

$$S = \gamma_{GS} - (\gamma_{GF} + \gamma_{FS}) \tag{24}$$

where $\gamma_{GS}$, $\gamma_{GF}$ and $\gamma_{FS}$ are the interfacial tensions of glass/surface, glass/fluid and fluid/surface, respectively [81]. A positive spreading coefficient indicates a stable film.

We note that the contact angle between fluid and glass was low, and that we may have observed a prewetting layer of fluid being trapped on the APTES-treated surfaces. Together, these drive us to the idea that $\gamma_{GF}$ and $\gamma_{FS}$ are probably small, meaning that $S$ is likely to be positive (equation (24)). Furthermore, it has been shown that for instable liquid films ($S < 0$) on soft surfaces, macroscopic dewetting occurs by nucleation and growth of a dry patch [65], phenomena not observed in our experiments. Thus, the lubricated contact seems to be energetically favourable and the film may be continuous; thereby any direct interactions between the surface and the glass sphere could be prevented.

The alternative explanation for force transmission in the presence of a fluid layer could be found in the confinement of the liquid. Although confined liquids are known to show a behaviour that differs significantly from their bulk behaviour, little research has been done on the exact effects of confinement on adhesion. At this stage, evidence lacks for coupling force transmission through the liquid layer to the confinement of the liquid. Further research is required to gain insight in this behaviour.

All together, this mechanism is able to directly explain the lower rate-dependence in the presence of a liquid as an effect of an increased interfacial mobility. A similar effect of lubrication on rate-dependence of adhesion has been reported before [26, 31]. Moreover, the mechanism does provide a plausible explanation for the course of the force trace. However, it relies on the assumption that forces can be transmitted through the mobile interfacial layer, either via chain penetration or via anomalous fluid behaviour induced by confinement of the liquid layer.

### Mechanism 2: Viscoelastic braking

The second model accounting for viscoelastic losses in wet adhesion arises when we take a closer look at the wet "crack" propagation. For this mechanism, we interpret the rim of the dark area as the result of a finite contact angle between a macroscopic droplet and the prewetted surrounding region (see the introduction of the previous mechanism). A propagation of the "wet crack" now resembles the motion of a contact line (see Figure 11b).

Effects of the movement of a contact line may drastically influence the (de)wetting behaviour: liquid droplets on soft solids can generate strong surface deformations below the contact line, resulting from a balance of surface tension and elastic forces [33, 82–85]. The vertical force due to the fluid surface tension, given by $f_0 = \gamma_F \sin\theta$, pulls up a "wetting ridge" around the contact line.[7] The height of this wetting ridge $l_r$ is of the order $\gamma_F/E_S$, where $E_S$ is the shear modulus of the soft solid. Using $E_S = E/3$ for incompressible solids, $E = 1\,\text{MPa}$ and $\gamma_F = 64\,\text{mN m}^{-1}$, we estimate $l_r = 0.19\,\mu\text{m}$.

For wetting experiments on soft solid surfaces, it has been shown that the movement of the contact line is accompanied by a movement of the wetting ridge, giving rise to energy dissipation in the viscoelastic solid [86, 87]. For a given driving force, contact line displacement then occurs at a speed lower than the speed measured on a non-deformable surface of similar surface energy and roughness. This phenomenon, called “viscoelastic braking”, may have such important consequences on the dynamic wetting behaviour that dissipation due to dislocation of the wetting ridge can dominate dissipation due to fluid movement [88].

Viscoelastic dissipation has been found to be related to the speed of the contact line $u$ in the following way [33, 83, 88]:

$$G \propto (u/u_0)^p \tag{25}$$

where $u_0$ and $p$ are constants. Note the striking similarity of equation (25) with the dissipation function describing the dependence of dry adhesion on crack propagation speed (equation (7)). Both models consider the overall mechanical response of the system to be dominated by the properties of the solid, and both models describe viscoelastic losses to result from high strain rates at the contact edge. Parallels between dissipation due to contact line motion and dry crack propagation have been drawn before in various studies [33, 82]. Estimates for $p$ range from 0.5 to 0.6, literature values for $u_0$ are in the range of 0.01 to $1\,\text{mm s}^{-1}$ [33]. In fact, $u_0$ is in a similar way related to energy dissipation as $v^*$: both are lower for "lossier" substrates [33], thus indicating a higher rate-dependence for lossier substrates. Note that estimates for $u_0$ are orders of magnitude higher than estimates for $v^*$, which typically range up to $0.4\,\mu\text{m s}^{-1}$ [27, 30, 31].

The above indicates that, in the wet adhesives, viscoelastic dissipation may have been induced by the movement of a wetting ridge. Our outcomes do show that peak adhesion increased with the wet "crack" propagation speed (see Figure 10), which is in line with equation (25). Again, we attempt to explain the force trace according to the mechanism.

(i) *Increasing force caused by dewetting and PDMS response:* We note that the dark area recedes with increasing speed up to the collapse (blue line in Figure 7). Since we have coupled the receding dark area to the displacement of a contact line, this motion should involve some form of dewetting. Apart from dewetting, forces may be incorporated in the motion of the wetting ridge via the elastic or viscous response of the material. Moreover, confinement of

[7] Note that for $\theta = 0$, there is no wetting ridge.

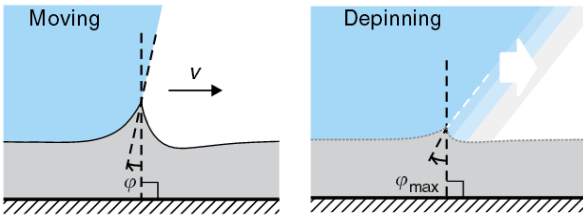


**Figure 12: Dynamics of a wetting ridge.** Obtained from Karpitschka et al. (2015) [89]. (**12a**) Displacement of the triple line is accompanied by a displacement of the wetting ridge, and causes a rotation $\varphi$ of the ridge. (**12b**) When the ridge is forced to tilt over its saturation rotation angle $\varphi_{max}$, the contact line depins from the ridge and surfs down the ridge.

the liquid may also induce additional deformation of the PDMS. It is difficult to assess the contributions of the different phenomena from the experimental data.

(ii) *Peak adhesive force at ridge saturation angle:* Recently, in a dynamic wetting experiment of a drop on a soft substrate, Karpitschka et al. [89] have found that the moving contact line induces a rotation of the wetting ridge, whose orientation angle is then dependent on the contact line velocity (see Figure 12a). For high contact line velocities, the rotation angle appears to reach a maximum, the "saturation" angle. Translating this to our experiments, taking into account the increasing speed of the contact line mentioned under (i), we note that this framework so far provides an explanation for the ridge orientation angle to reach its saturation rotation angle. It should be noted that the analogy with the experiments performed in ref. [89] is limited for the fact that our experiments concerned a dewetting motion and that we impose our system to an external force, i.e. the tensile force acting on the liquid bridge may have caused an imbalance in the relation between contact angle and contact line speed.

(iii) *Force drop caused by depinning:* The observed drop in force might follow from a dynamical depinning of the contact line from the ridge. Such a depinning is in line with the "collapse" of the area of the macroscopic fluid layer (see Figure 7) that accompanies the force drop. A theoretical explanation for this depinning is given in ref. [89] and reads as follows: when the force applied on the contact causes the contact angle to exceed its saturation angle, the contact line dynamically depins from the ridge, surfing it until a new wetting ridge is formed (see Figure 12b). Such a stick-slip motion has been reported before [90, 91]. As a slip movement may proceed without a displacement of the wetting ridge, no viscoelastic dissipation would be involved in the motion [92], which corresponds to the drop in force conform observations. Also, viscoelastic braking will not occur during a slip motion, allowing the

contact line to move with a high speed conform observations (Figure 7). Repinning of the contact line may explain the end of the force drop at a non-zero adhesive force. It should be noted that this explanation can not be translated to the force drop observed in ref. [71], where rigidity of the surfaces will have prevented the formation of a wetting ridge.

(iv) *Decreasing force when capillary bridge is being stretched:* It is tempting to use the same convenient explanation for the final part of the force trace as we did for the previous mechanism. However, if we assume that viscoelastic braking has a significant effect on the measured forces, we need to take this contribution also into account in the last part. Regarding the high speed of the contact line in this part of detachment (see Figure 7), viscoelastic dissipation due to viscous braking should *increase* in this stage, according to our reasoning. Although the perimeter of the contact area may have decreased, and with that the length of the contact line and in turn the volume of material deformed, this decrease seems to be minor compared to the increase in speed.

In order to couple the decrease in rate-dependence to the presence of a liquid, we revisit equation (25). The similarity between equation (25) and equation (7) allows us to use these equations to compare rate-dependence between wet and dry adhesion. Comparison reveals that $n$ and $p$ are both found between 0.5 and 0.6 [29, 33], indicating that both empirical laws describing energy dissipation take the same form. While $v^*$ usually takes values up to $0.4\,\mu m\,s^{-1}$ for elastomers [27, 30, 31], values for $u_0$ range up to $mm\,s^{-1}$ [33]. According to this mechanism, a similar relation between "crack" propagation speed and adhesion would be expected between wet and dry adhesion experiments, albeit with a lower velocity dependence in the presence of a fluid layer.

Hence, the lower rate-dependence of wet adhesion can also be explained with viscoelastic braking. However, effects expected from viscoelastic braking are in direct contradiction to what we see in the last part of the force trace. Furthermore, the plausibility of this mechanism is determined by the interpretation of the observed wetting phenomena, i.e. the plausibility of a moving contact line.

In summary, a low rate-dependence in wet adhesion may have resulted from viscoelastic losses, but the exact mechanism for these losses can not be extracted from our experiments. A lower rate-dependence as an effect of increased interfacial mobility provides an explanation for all events that we observed in the force trace, but depends on force transmission through the liquid layer. A different explanation may be found in viscoelastic braking, but only if the liquid layer has actually pulled up a wetting ridge and even then, the final slow decrease in force is in contradiction with the proposed framework. A comparison of the proposed mechanisms reveals that while the first mechanism only holds for confined liquids, viscoelastic braking would occur also for liquids showing their bulk behaviour. It should be noted that a combination of the two mechanisms can not be excluded: when a liquid is confined between the PDMS surface and rigid indenter, it may also pull up a wetting ridge at

the contact line. Further research is required to assess the respective contributions of the two mechanisms.

## 4.3 Viscoelastic dissipation in insect adhesion

Our results suggest that viscous dissipation in the liquid does not have a dominant effect when an interfacial liquid is in elastic confinement, and that rate-dependent behaviour may be determined by viscoelastic losses in the solid.

If we revisit the insect wet adhesive mechanism with these new insights, the first thing to note is that the thickness of the secretion layer is in the range of nanometers [9]. This means that the liquid is most likely in a comparable elastic confinement as the liquid in our adhesive system [70]. Continuing this line of thought, it seems to be plausible that, even when contact is mediated by a fluid layer, viscoelastic dissipation can take place in the pad as the overall response will be dominated by the behaviour of the footpad.

Thus, instead of the liquid film *causing* rate-dependence via its viscous component, we rather believe that the secretion allows the animal to *reduce* rate-dependence by minimizing viscoelastic losses in the footpad. A strong velocity-dependence of adhesion of the animal feet may have negative consequences: during locomotion, for example, fast detachment would require additional work and might eventually lead to damage of the pad. Minimizing rate-dependence via the secretion of a liquid could be a valuable tool to control detachment.

It has been stated that solid-solid interactions between footpad and surface can not be excluded in wet adhesion [9], which supports the idea of a crack that propagates upon adhesive failure. If this is the case, we might consider the fluid layer to decrease rate-dependence of adhesion by minimizing viscoelastic losses near the crack tip.

On the other hand, a low rate-dependence of insect adhesion [12] is in line with viscoelastic braking involving a small wetting ridge. Considering the low contact angle of the fluid with the pad (receding angle about $9^\circ$ [93]), the vertical component of surface tension will be small, suggesting the presence of a small wetting ridge. However, viscoelastic braking would require an actual displacement of the contact line over the pad, thus either a local dewetting of the pad during detachment which is unlikely [94], or partial wetting of the secretion film on the pad, similar to the partial wetting as described above.

Although this research has led to the suggestion of two distinct mechanisms that may account for viscoelastic dissipation in the presence of a liquid, we can not translate one of them directly to wet adhesion of animals. In order to find out the exact mechanism that nature has designed for wet adhesives, further experimental research is required.

# 5 | Future research

From the previous section, it has come clear that our understanding of the dissipation processes in wet adhesion is not yet complete. During this study, several opportunities for future research were encountered which will be discussed in the following section. The section starts with discussing several aspects of this research that have limited us in the interpretation of the observed phenomena. These limitations are accompanied by suggestions for improvement. The section ends with new questions that have emerged from this project, both in the research field of physical chemistry as in the world of biomechanics.

## 5.1 Research limitations

Starting with the dry adhesion, we note that consistency between the simple model system and literature data is a prerequisiste for our outcomes to be related to the work done on adhesion of soft solids. However, our results for rate-dependence of PDMS showed significant discrepancy with literature values. Three major limitations have been identified that may contribute to a discrepancy between our dry adhesion outcomes and literature.

First, we note that a synchronization of contact area data with force data was not possible for relatively high retraction speeds. Our setup was hence not suited to relate adhesion to crack propagation speed for these high retraction speeds. An effect of this emerged when we assessed rate-dependence using equation (9), where we used the outcome of only three retraction speeds for fitting. Proper synchronization could have been performed with lower frame rates, but this would have led to a decreased resolution of the contact data. Addressing the signal transfer problem would facilitate model fitting over a larger extent of the experimental data.

Second, we mention the procedure for obtaining force-displacement data. Our method for determining zero displacement is somewhat arbitrary and prone to errors. This will have had an impact on fitting with the Barquins and Maugis fitting procedure. An improvement in this respect could be the use of a displacement transducer [27, 55].

Third, the applied methods for quantifying rate-dependence raise questions. Fitting equation (9) was limited because of the amount of data that could be used for crack propagation speeds, whereas the Barquins and Maugis fitting procedure was strongly dependent on starting values and set boundaries as mentioned in discussion. If we take into account the two comments above, we may ideally

have used three input states ($\delta$, $P$ and $a$) for the Barquins and Maugis fitting procedure. An additional independent parameter would improve the quality of the fits. Nevertheless, errors may still have diverged for higher retraction speeds and a strong interdependence of the estimates may have remained. Ideally, $G$ is calculated over the duration of the experiments, using accurate measurements of $\delta$, $P$ and $a$. This is the method often applied in literature [26, 27, 31, 61]. Then, by determining the crack propagation speed over the duration of the experiment, $n$, $G_0$ and $v^*$ can be determined.

For the analysis of wet adhesion data, the major limiting factors were found in visualisation aspects.

A proper indication of the fluid layer thickness is the key to detailed analysis of wet adhesion measurements. The film thickness is determinant with respect to: estimating viscosity effects, assessing confinement and estimating occurrence of chain penetration. However, dynamic measurements of fluid film thicknesses in the nanometer range are challenging, especially for dynamic measurements. IRM measurements have been performed to measure fluid thickness in static contacts [9]. A prerequisite was that the droplet was located on a flat, undeformed surface. In our current setup, non-flatness and deformation of the PDMS would influence the measured profile. A more sophisticated approach was used by Wexler et al. (2014) [95] for determining the *z*-profile of a droplet confined between two soft flat substrates. By making use of interferometry in combination with a high-magnification confocal *z* stack the droplet profile could be reproduced. A more simple approach could be obtained by slightly changing our setup. If a glass coverslip is used in combination with an elastomeric lens, one might use IRM to view the contact area through the coverslip. In this way, the droplet thickness can be determined from the interference profile.

Furthermore, the quality of the top-view images was limited. Upon spreading a droplet over the treated PDMS, we observed different regions. Although we made phenomenological interpretations of these observed regions, little data was available to verify these interpretations. The second mechanism proposed for viscoelastic dissipation depends extensively on the quality of our interpretations of the wetting phenomena.

## 5.2 New questions

This work has opened up new hypotheses for the origin of viscoelastic dissipation in the presence of a liquid layer.

A significant part of this work was focussed on finding the phenomenon underlying rate-dependence in the adhesion of the artificial system. We identified two possible mechanisms (see discussion), none of which could fully explain the observed phenomena. In order to gain more insight in the dynamics of adhesion of our system, the following experimental parameters could be changed:

(i) *Equilibration time during load:* Following equation (20), changing the equilibration time during load should result in different film thicknesses. Energy

dissipation as a result of crack propagation through the fluid layer requires the layer to be in elastic confinement or to allow chain penetration. In either case, a certain minimal fluid thickness would prevent this mechanism from dissipating energy. Since energy dissipation in viscoelastic braking will also occur for liquid layers of macroscopic thickness, different equilibration times can be used to distinguish between the two mechanisms.

(ii) *Rigidity of the PDMS:* A soft solid with a higher elastic modulus will be deformed less by surface tension of a contacting droplet. Furthermore, it has been shown that the cross-linking density of PDMS is related to the maximum displacement speed of the wetting ridge [88]. If viscoelastic braking dominates the displacement of the alleged contact line in wet adhesives, a similar relation between rigidity and contact line speed should be present. Eventually, one might even use a setup that constitutes of a surface and an indenter that are both rigid. In analogy to the experiments performed by Zhang et al. [71], a splitting procedure can be used to assess the effect of elastic confinement on dynamic adhesion. An attempt could be made to relate this elastic confinement to the transition from a continuously decreasing force to a shrinking release force (see ref. [71]).

(iii) *Chemistry of surface or liquid:* Changing the contact angle between the liquid and the surface should have an effect on the height of the wetting ridge that is pulled up around the contact line. In the extreme case, a completely wetting fluid ($\theta = 0$) would not pull up a ridge. In turn, this may have effect on the viscoelastic dissipation and thus on rate-dependence.

Extending the outcomes towards a broader field of soft solids and biomechanics raises curiosity. For example, in earlier research it was found that adhesion of insect footpads is an order of magnitude higher on several polymeric surfaces than on glass and mica.[1] It would be interesting to test the same dependence of the adhesive behaviour of fluid-mediated PDMS adhesion on polymer surfaces. Furthermore, the adhesion of insect pads is strongly dependent on the shear force applied on the footpad [12]. The effect of a combination of parallel and normal forces could also be tested on the artificial system. Fluid depletion is an interesting additional variable when testing this.

[1] J.H. Dirks, unpublished data

# 6 | Conclusion

The presence of a thin fluid layer between a rigid indenter and a soft solid decreased the rate-dependence of adhesion. The rate-dependence was independent of the viscosity of the contact-mediating fluid, which appeared to be in "elastic confinement". Our results suggest that the rate-dependence of these "wet adhesives" was caused by dissipative phenomena in the viscoelastic solid rather than by viscous dissipation in the liquid. Two mechanisms may explain solid-dominated viscoelastic dissipation in wet adhesion.

First, the wet adhesive contact may be akin to a dry contact with an increased interfacial mobility. The liquid layer induces a lubrication effect, which reduces viscoelastic dissipation in the solid caused by high strain rates at the tip of the propagating crack, thereby reducing the rate-dependence of adhesion. However, it is unclear whether force could be transmitted through the interfacial layer. We identified two possible ways for this force transmission: chain penetration or anomalous fluid behaviour resulting from confinement. Notwithstanding, we have no evidence for chain penetration through the layer, nor have extensive studies been performed on the effect of liquid confinement on adhesion.

Second, the movement of a wetting ridge may cause viscoelastic dissipation via "viscoelastic braking". The surface tension of liquids is known to cause local deformation of soft solids around the contact line, whose movement can trigger a viscoelastic response. In wet adhesion experiments, a movement of the alleged contact line was observed, which would be accompanied by a displacement of the wetting ridge. The velocity of the contact line around the moment of peak adhesion was found to increase with retraction speed, and the accompanied wetting ridge movement may have led to increased dissipation in the solid by inducing increasing strain-rates. Notwithstanding, this mechanism is not yet able to explain the final part of the force trace, where a fast movement of the contact line was accompanied by a decrease in force.

We anticipate that also in insect adhesion, rate-dependence may arise from viscoelastic dissipation in the insect footpad rather than from viscous effects in the liquid, as the secreted fluid mediating the contact is in a similar confinement. However, the exact way in which rate-dependence is induced remains unclear both in the model system and in insect pads, and requires further investigation. The model system appears to be a promising tool for studying and understanding the physical mechanisms underlying the rate-dependence in insect pads, and wet soft adhesives in general.

# References


[1] L. Frantsevich and S. Gorb. Structure and mechanics of the tarsal chain in the hornet, *Vespa crabro* (Hymenoptera: Vespidae): implications on the attachment mechanism. *Arthropod structure & development*, 33(1):77–89, 2004.

[2] W. Federle and T. Endlein. Locomotion and adhesion: dynamic control of adhesive surface contact in ants. *Arthropod Structure & Development*, 33(1):67–75, 2004.

[3] S. N. Gorb, M. Sinha, A. Peressadko, K. A. Daltorio, and R. D. Quinn. Insects did it first: a micropatterned adhesive tape for robotic applications. *Bioinspiration & biomimetics*, 2(4):S117, 2007.

[4] J.-H. Dirks, C. J. Clemente, and W. Federle. Insect tricks: two-phasic foot pad secretion prevents slipping. *Journal of the Royal Society Interface*, 7(45):587–593, 2010.

[5] J.-H. Dirks and W. Federle. Fluid-based adhesion in insects–principles and challenges. *Soft Matter*, 7(23):11047–11053, 2011.

[6] H. Power. Experimental philosophy in three books: Containing new experiments microscopical. *Mercurial, Magnetical (London: T. Roycroft for John Martin and James Allestry, 1664)*, 6(7), 1664.

[7] T. West. Xxv. the foot of the fly; its structure and action: elucidated by comparison with the feet of other insects. *Transactions of the Linnean Society of London*, 23 (2):393–421, 1861.

[8] K. Autumn, M. Sitti, Y. A. Liang, A. M. Peattie, W. R. Hansen, S. Sponberg, T. W. Kenny, R. Fearing, J. N. Israelachvili, and R. J. Full. Evidence for van der Waals adhesion in gecko setae. *Proceedings of the National Academy of Sciences*, 99(19): 12252–12256, 2002.

[9] W. Federle, W. Barnes, W. Baumgartner, P. Drechsler, and J. Smith. Wet but not slippery: boundary friction in tree frog adhesive toe pads. *Journal of The Royal Society Interface*, 3(10):689–697, 2006.

[10] S. F. Geiselhardt, W. Federle, B. Prüm, S. Geiselhardt, S. Lamm, and K. Peschke. Impact of chemical manipulation of tarsal liquids on attachment in the Colorado potato beetle, *Leptinotarsa decemlineata*. *Journal of insect physiology*, 56(4):398–404, 2010.

[11] J.-H. Dirks and W. Federle. Mechanisms of fluid production in smooth adhesive pads of insects. *Journal of The Royal Society Interface*, 2011.

[12] D. Labonte and W. Federle. Rate-dependence of 'wet'biological adhesives and the function of the pad secretion in insects. *Soft matter*, 11(44):8661–8673, 2015.

[13] S. B. Emerson and D. Diehl. Toe pad morphology and mechanisms of sticking in frogs. *Biological Journal of the Linnean Society*, 13(3):199–216, 1980.

[14] G. Walker. Adhesion to smooth surfaces by insects a review. *International Journal of Adhesion and Adhesives*, 13(1):3–7, 1993.

[15] M. G. Langer, J. P. Ruppersberg, and S. Gorb. Adhesion forces measured at the level of a terminal plate of the fly's seta. *Proceedings of the Royal Society of London B: Biological Sciences*, 271(1554):2209–2215, 2004.

[16] W. J. P. Barnes. Functional morphology and design constraints of smooth adhesive pads. *MRS bulletin*, 32(06):479–485, 2007.

[17] J.-H. Dirks. Physical principles of fluid-mediated insect attachment-shouldn t insects slip? *Beilstein journal of nanotechnology*, 5(1):1160–1166, 2014.

[18] J. S. Edwards and M. Tarkanian. The adhesive pads of Heteroptera: a re-examination. In *Proceedings of the Royal Entomological Society of London. Series A, General Entomology*, volume 45, pages 1–5. Wiley Online Library, 1970.

[19] A. Dixon, P. Croghan, and R. Gowing. The mechanism by which aphids adhere to smooth surfaces. *Journal of Experimental Biology*, 152(1):243–253, 1990.

[20] B. Andreotti, O. Bäumchen, F. Boulogne, K. E. Daniels, E. R. Dufresne, H. Perrin, T. Salez, J. H. Snoeijer, and R. W. Style. Solid capillarity: when and how does surface tension deform soft solids? *Soft matter*, 12(12):2993–2996, 2016.

[21] R. W. Style, C. Hyland, R. Boltyanskiy, J. S. Wettlaufer, and E. R. Dufresne. Surface tension and contact with soft elastic solids. *Nature communications*, 4, 2013.

[22] R. W. Style, R. Boltyanskiy, B. Allen, K. E. Jensen, H. P. Foote, J. S. Wettlaufer, and E. R. Dufresne. Stiffening solids with liquid inclusions. *Nature Physics*, 11(1): 82–87, 2015.

[23] A. Fogden and L. R. White. Contact elasticity in the presence of capillary condensation: I. The nonadhesive Hertz problem. *Journal of Colloid and Interface Science*, 138(2):414–430, 1990.

[24] J.-B. Valsamis and P. Lambert. Axial capillary forces (dynamics). In *Surface Tension in Microsystems*, pages 137–177. Springer, 2013.

[25] M. Barquins and D. Maugis. Tackiness of elastomers. *The Journal of Adhesion*, 13 (1):53–65, 1981.

[26] K. R. Shull, D. Ahn, W.-L. Chen, C. M. Flanigan, and A. J. Crosby. Axisymmetric adhesion tests of soft materials. *Macromolecular Chemistry and Physics*, 199(4): 489–511, 1998.

[27] D. Ahn and K. R. Shull. JKR studies of acrylic elastomer adhesion to glassy polymer substrates. *Macromolecules*, 29(12):4381–4390, 1996.

[28] M. A. Meyers and K. K. Chawla. *Mechanical behavior of materials*, volume 2. Cambridge university press Cambridge, 2009.

[29] M. Barquins. Adhesive contact and kinetics of adherence between a rigid sphere and an elastomeric solid. *International Journal of Adhesion and Adhesives*, 3(2):71–84, 1983.

[30] D. Ahn and K. R. Shull. Effects of methylation and neutralization of carboxylated poly (n-butyl acrylate) on the interfacial and bulk contributions to adhesion. *Langmuir*, 14(13):3637–3645, 1998.

[31] D. Ahn and K. R. Shull. Effects of substrate modification on the interfacial adhesion of acrylic elastomers. *Langmuir*, 14(13):3646–3654, 1998.

[32] K. R. Shull. Contact mechanics and the adhesion of soft solids. *Materials Science and Engineering: R: Reports*, 36(1):1–45, 2002.

[33] M. Shanahan and A. Carre. Viscoelastic dissipation in wetting and adhesion phenomena. *Langmuir*, 11(4):1396–1402, 1995.

[34] G. L. Lake and A. Stevenson. *On the Mechanics of Peeling*, volume Adhesion 6. Applied Science Publishers, 1982.

[35] G. J. La. Proceedings of the International Adhesion Conference, Nottingham 1984. pages 22.1–22.4, London, 1984. The Plastics and Rubber Institute, Londen.

[36] H. Brown. Chain pullout and mobility effects in friction and lubrication. *Science*, 263:11, 1994.

[37] B.-m. Z. Newby, M. K. Chaudhury, and H. R. Brown. Macroscopic evidence of the effect of interfacial slippage on adhesion. *Science*, 269(5229):1407, 1995.

[38] F. D. Blum, B. C. Gandhi, D. Forciniti, and L. R. Dharani. Effect of surface segmental mobility on adhesion of acrylic soft adhesives. *Macromolecules*, 38(2):481–487, 2005.

[39] S. Gorb, Y. Jiao, and M. Scherge. Ultrastructural architecture and mechanical properties of attachment pads in *Tettigonia viridissima* (*Orthoptera Tettigoniidae*). *Journal of Comparative Physiology A*, 186(9):821–831, 2000.

[40] Z. Wang. Polydimethylsiloxane mechanical properties measured by macroscopic compression and nanoindentation techniques. Master's thesis, University of South Florida, 2011.

[41] X. Q. Brown, K. Ookawa, and J. Y. Wong. Evaluation of polydimethylsiloxane scaffolds with physiologically-relevant elastic moduli: interplay of substrate mechanics and surface chemistry effects on vascular smooth muscle cell response. *Biomaterials*, 26(16):3123 – 3129, 2005. ISSN 0142-9612.

[42] F. Carrillo, S. Gupta, M. Balooch, S. J. Marshall, G. W. Marshall, L. Pruitt, and C. M. Puttlitz. Nanoindentation of polydimethylsiloxane elastomers: Effect of crosslinking, work of adhesion, and fluid environment on elastic modulus. *Journal of Materials Research*, 20:2820–2830, 10 2005.

[43] I. Scholz, W. Baumgartner, and W. Federle. Micromechanics of smooth adhesive organs in stick insects: pads are mechanically anisotropic and softer towards the adhesive surface. *Journal of Comparative Physiology A*, 194(4):373–384, 2008.

[44] P. P. Goodwyn, A. Peressadko, H. Schwarz, V. Kastner, and S. Gorb. Material structure, stiffness, and adhesion: why attachment pads of the grasshopper (*Tettigonia viridissima*) adhere more strongly than those of the locust (*Locusta migratoria*)(Insecta: Orthoptera). *Journal of Comparative Physiology A*, 192(11):1233–1243, 2006.

[45] A. V. Birn-Jeffery. Unpublished data.

[46] A. Mata, A. J. Fleischman, and S. Roy. Characterization of polydimethylsiloxane (pdms) properties for biomedical micro/nanosystems. *Biomedical microdevices*, 7 (4):281–293, 2005.

[47] N.-S. Cheng. Formula for the viscosity of a glycerol-water mixture. *Industrial & Engineering chemistry research*, 47(9):3285–3288, 2008.

[48] C. S. Miner and N. Dalton. *Glycerol*, volume 117. Reinhold Pub. Corp., 1953.

[49] C. Vicente, P. Andre, and R. Ferreira. Simple measurement of surface free energy using a web cam. *Revista Brasileira de Ensino de Física*, 34(3):1–5, 2012.

[50] B. E. Slentz, N. A. Penner, E. Lugowska, and F. Regnier. Nanoliter capillary electrochromatography columns based on collocated monolithic support structures molded in poly (dimethyl siloxane). *Electrophoresis*, 22(17):3736–3743, 2001.

[51] *Analog Sensor Data Sheet, D12 fibre optic sensor*. Philtec, INC., Annapolis, MD, USA.

[52] E. Kroner, R. Maboudian, and E. Arzt. Adhesion characteristics of pdms surfaces during repeated pull-off force measurements. *Advanced Engineering Materials*, 12 (5):398–404, 2010.

[53] R Development Core Team. *R: A Language and Environment for Statistical Computing*. R Foundation for Statistical Computing, Vienna, Austria, 2008. ISBN 3-900051-07-0.

[54] W. Rasband. *ImageJ*. U. S. National Institutes of Health, Bethesda, Maryland, USA, 1997-2016.

[55] D. Maugis and M. Barquins. *Fracture Mechanics and Adherence of Viscoelastic Solids*. Springer US, Boston, MA, 1980.

[56] K. Johnson, K. Kendall, and A. Roberts. Surface energy and the contact of elastic solids. In *Proceedings of the Royal Society of London A: Mathematical, Physical and Engineering Sciences*, volume 324, pages 301–313. The Royal Society, 1971.

[57] S.-H. Choi and B.-M. Z. Newby. Suppress polystyrene thin film dewetting by modifying substrate surface with aminopropyltriethoxysilane. *Surface Science*, 600(6):1391 – 1404, 2006.

[58] K. L. Mittal. *Silanes and Other Coupling Agents, Volume 4*. CRC Press, Taylor & Francis group, 2007.

[59] D. Maugis. Adherence of elastomers: fracture mechanics aspects. *Journal of Adhesion Science and Technology*, 1(1):105–134, 1987.

[60] A. J. Crosby and K. R. Shull. Adhesive failure analysis of pressure-sensitive adhesives. *Journal of Polymer Science Part B: Polymer Physics*, 37(24):3455–3472, 1999.

[61] U. Abusomwan and M. Sitti. Effect of retraction speed on adhesion of elastomer fibrillar structures. *Applied Physics Letters*, 101(21):211907, 2012.

[62] J. Deuschle, S. Enders, and E. Arzt. Surface detection in nanoindentation of soft polymers. *Journal of Materials Research*, 22(11):3107–3119, 2007.

[63] G. P. Association et al. *Physical properties of glycerine and its solutions*. Glycerine Producers' Association, 1963.

[64] B. Francis and R. Horn. Apparatus-specific analysis of fluid adhesion measurements. *Journal of Applied Physics*, 89(7):4167–4174, 2001.

[65] P. Martin and F. Brochard-Wyart. Dewetting at soft interfaces. *Physical review letters*, 80(15):3296, 1998.

[66] S. Granick. Motions and relaxations of confined liquids. *Science*, 253:1374–9, 1991.

[67] S. Patil, G. Matei, A. Oral, and P. M. Hoffmann. Solid or liquid? solidification of a nanoconfined liquid under nonequilibrium conditions. *Langmuir*, 22(15):6485–6488, 2006.

[68] S. H. Khan, G. Matei, S. Patil, and P. M. Hoffmann. Dynamic solidification in nanoconfined water films. *Physical review letters*, 105(10):106101, 2010.

[69] S. Leroy and E. Charlaix. Hydrodynamic interactions for the measurement of thin film elastic properties. *Journal of Fluid Mechanics*, 674:389–407, 2011.

[70] R. Villey, E. Martinot, C. Cottin-Bizonne, M. Phaner-Goutorbe, L. Léger, F. Restagno, and E. Charlaix. Effect of surface elasticity on the rheology of nanometric liquids. *Physical review letters*, 111(21):215701, 2013.

[71] X. Zhang, X. Yi, S.-U. Ahmed, M. Kosinskiy, Y. Liu, and J. Schaefer. Dynamic contact model based on meniscus adhesion for wet bio-adhesive pads: Simulation experiments. *Tribology Transactions*, 53(2):280–287, 2010.

[72] D. I. Bower. *An introduction to polymer physics*. Cambridge University Press, 2002.

[73] J. Maas, M. Cohen Stuart, F. Leermakers, and N. Besseling. Wetting transition in a polymer brush: polymer droplet coexisting with two film thicknesses. *Langmuir*, 16 (7):3478–3481, 2000.

[74] M. Müller and L. G. MacDowell. Wetting of polymer liquids: Monte carlo simulations and self-consistent field calculations. *Journal of Physics: Condensed Matter*, 15(19): R609, 2003.

[75] A. Johner and C. M. Marques. Can a polymer brush trap a wetting layer? *Phys. Rev. Lett.*, 69:1827–1830, Sep 1992.

[76] F. Brochard-Wyart, J. M. Di Meglio, D. Quére, and P. G. De Gennes. Spreading of nonvolatile liquids in a continuum picture. *Langmuir*, 7(2):335–338, 1991.

[77] D. Bonn and D. Ross. Wetting transitions. *Reports on Progress in Physics*, 64(9): 1085, 2001.

[78] D. Bonn, E. Bertrand, N. Shahidzadeh, K. Ragil, H. Dobbs, A. Posazhennikova, D. Broseta, J. Meunier, and J. Indekeu. Complex wetting phenomena in liquid mixtures: frustrated-complete wetting and competing intermolecular forces. *Journal of Physics: Condensed Matter*, 13(21):4903, 2001.

[79] D. Maugis and M. Barquins. Adhesive contact of sectionally smooth-ended punches on elastic half-spaces: theory and experiment. *Journal of Physics D: Applied Physics*, 16(10):1843, 1983.

[80] J. N. Israelachvili. *Intermolecular and surface forces: revised third edition*. Academic press, 2011.

[81] A. Martin, A. Buguin, and F. Brochard-Wyart. Dewetting nucleation centers at soft interfaces. *Langmuir*, 17(21):6553–6559, 2001.

[82] M. E. Shanahan and A. Carre. Anomalous spreading of liquid drops on an elastomeric surface. *Langmuir*, 10(6):1647–1649, 1994.

[83] A. Carre and M. E. Shanahan. Direct evidence for viscosity-independent spreading on a soft solid. *Langmuir*, 11(1):24–26, 1995.

[84] A. Marchand, S. Das, J. H. Snoeijer, and B. Andreotti. Contact angles on a soft solid: from young's law to neumann's law. *Physical review letters*, 109(23):236101, 2012.

[85] R. W. Style, R. Boltyanskiy, Y. Che, J. Wettlaufer, L. A. Wilen, and E. R. Dufresne. Universal deformation of soft substrates near a contact line and the direct measurement of solid surface stresses. *Physical review letters*, 110(6):066103, 2013.

[86] D. Long, A. Ajdari, and L. Leibler. How do grafted polymer layers alter the dynamics of wetting? *Langmuir*, 12(6):1675–1680, 1996.

[87] M. Shanahan. The spreading dynamics of a liquid drop on a viscoelastic solid. *Journal of Physics D: Applied Physics*, 21(6):981, 1988.

[88] A. Carré and M. E. Shanahan. Effect of cross-linking on the dewetting of an elastomeric surface. *Journal of Colloid and Interface Science*, 191(1):141 – 145, 1997.

[89] S. Karpitschka, S. Das, M. Van Gorcum, H. Perrin, B. Andreotti, and J. Snoeijer. Droplets move over viscoelastic substrates by surfing a ridge. *Nature communications*, 6, 2015.

[90] T. Kajiya, A. Daerr, T. Narita, L. Royon, F. Lequeux, and L. Limat. Advancing liquid contact line on visco-elastic gel substrates: stick-slip vs. continuous motions. *Soft Matter*, 9(2):454–461, 2013.

[91] T. Kajiya, P. Brunet, L. Royon, A. Daerr, M. Receveur, and L. Limat. A liquid contact line receding on a soft gel surface: dip-coating geometry investigation. *Soft Matter*, 10(44):8888–8895, 2014.

[92] H. Bodiguel, F. Doumenc, and B. Guerrier. Stick- slip patterning at low capillary numbers for an evaporating colloidal suspension. *Langmuir*, 26(13):10758–10763, 2010.

[93] J.-H. Dirks. *Mechanisms of fluid-based adhesion in insects*. PhD thesis, University of Cambridge, 2010.

[94] P. Drechsler and W. Federle. Biomechanics of smooth adhesive pads in insects: influence of tarsal secretion on attachment performance. *Journal of Comparative Physiology A*, 192(11):1213–1222, 2006.

[95] J. S. Wexler, T. M. Heard, and H. A. Stone. Capillary bridges between soft substrates. *Physical review letters*, 112(6):066102, 2014.

# Appendix

## Recordings

Link to videos:

https://www.dropbox.com/sh/9i765x1g8en51vc/AACpuN3F7u0zw4JRd3r8ufXFa?dl=0

The videos correspond to the force traces depicted in Figure 5. For both the dry and the wet adhesion experiment, a side-view recording and a top-view recording are given.

**Description:**

*Dry_topview*: Initially, PDMS deformation by the sphere is visible in the top-left part of the screen. As retraction proceeds, we note two things: (i) a darker area around the circular deformation starts to appear and (ii) the circular deformation decreases in size. Eventually, a white ring is visible that clearly distinguishes the two areas. Both regions can be attributed to PDMS deformation. The inner region shows the deformation caused by indentation of the sphere. The outer region is an upwards deformation caused by the adhesive force in the contact zone. After 850 frames, the sphere detaches from the PDMS.

*Dry_sideview*: In the lower part of the screen, the spherical indenter is visible. A reflection of the sphere in the PDMS can be seen just above the top of the sphere. A detachment seems to occur around frame 850.

*Wet_topview*: The dark area slowly recedes during the first 570 frames. Then, the area "collapses" occurs between frame 570 and 600. After frame 600, the dark area again decreases steadily, but faster than in the initial stage.

*Wet_sideview*: The sphere is again visible in the lower part of the image. The fluid layer can be distinguished on top of the sphere. Upon retraction, the meniscus of the fluid appears to move inwards. This movement of the meniscus occurs faster after frame 570.